SEDIMENT DYNAMICS AND STRATIGRAPHIC ARCHITECTURE OF A LOWER SILURIAN STORM-DOMINATED CARBONATE RAMP, ANTICOSTI ISLAND, QUÉBEC, CANADA

FRANÇOIS CLAYER

Thèse soumise à la
Faculté des études supérieures et postdoctorales
Université d'Ottawa
en vue de l'obtention de la maîtrise ès sciences en
Sciences de la Terre

Centre géoscientifique d'Ottawa-Carleton
et
Université d'Ottawa
Ottawa, Canada

Thesis submitted to the
Faculty of Graduate and Postdoctoral Studies
University of Ottawa
in partial fulfillment of the requirements for the
M.Sc. degree in Earth Sciences

Ottawa-Carleton Geoscience Center
and
University of Ottawa
Ottawa, Canada

Résumé

La succession du Llandovery inférieur à la limite entre les formations de Jupiter et de Chicotte sur l'île d'Anticosti, Québec, nous permet d'étudier la dynamique sédimentaire et l'architecture stratigraphique d'une rampe carbonatée dominée par les tempêtes. La rampe paléo-tropicale d'Anticosti était soumise à une lente subsidence et a donc enregistré les fluctuations subtiles du niveau marin pendant un épisode glaciaire du Télychien inférieur. Trois associations de faciès, regroupant neuf faciès, ont été reconnues le long de la ceinture d'affleurement orientée E-W, du sommet à la base : (FA-1) faciès carbonatés à encrinites, (FA-2) faciès mixtes silico-carbonatés, et (FA-3) faciès carbonatés sans encrinites. Ces tempestites de la rampe médiane représentent une déposition majoritairement lors d'épisodes de haute énergie caractérisés par des stratifications à faible angle (« *hummocky cross stratification* »), de grandes rides de vague, des gouttières (« *gutter casts* »), et des dépôts de courants gravitaires liés à l'action des vagues.

Des changements spatiaux et temporels dans l'apport en sédiments silico-clastiques impliquent des environnements de dépôts marginaux dans les sections de l'est et un changement dans le régime climatique passant d'aride à humide. Le dépôt du Chicotte marque un changement majeur dans la faune benthique avec la domination des crinoïdes engendrée par l'augmentation de l'influx silico-clastique, des changements rapides du niveau marin et du substrat. La reconnaissance d'une séquence majeure transgressive-régressive (TR), subdivisée en cycles à l'échelle métrique, permet une corrélation E-W de haute résolution. Le développement de notre séquence et de nos cycles TR est contrôlé par la glacio-eustasie où la séquence majeure est du 4ème ordre (~400 Ka) alors que les cycles sont du 5ème et/ou 6ème ordre (~100 Ka). Néanmoins, des surfaces d'érosion au sein des tempestites proximales reflètent des paléo-côtes rocheuses lors de baisses forcées du niveau marin. Afin d'expliquer cette architecture stratigraphique, un modèle de rampe carbonatée ouverte est proposé avec un profile concave et une rampe interne restreinte et pentue en équilibre avec une ligne de rivage de haute énergie.

Abstract

The upper Llandovery succession across the Jupiter-Chicotte formational contact on Anticosti Island, Québec, allows us to study the sediment dynamics and stratigraphic architecture of a storm-dominated, carbonate ramp. The Anticosti paleotropical ramp was slowly subsiding and recording significant changes in sea level in a far field glacial setting during the early Telychian. Three facies associations, grouping nine facies, are recognized along the E-W outcrop belt, and from top to bottom as the: (FA-1) encrinitic carbonate facies, (FA-2) mixed siliciclastic and carbonate facies, and (FA-3) non-encrinitic carbonate facies. These mid to outer ramp sediments represent deposition mostly from episodic, high-energy storm events as evidenced by hummocky cross-stratification, large wave ripples, gutter casts, and wave-enhanced sediment-gravity flow deposits.

Spatial and temporal changes in siliciclastic content imply basin margin depositional environments in the eastern sections and change in climate regime from arid to humid conditions. The Chicotte deposition marks a major faunal change with the domination of crinoids triggered by increasing siliciclastic supply, rapid sea level fluctuations and change in substrates. The recognition of one major transgressive-regressive (TR) sequence subdivided in distinct meter-scale cycles allows a high resolution E-W correlation. The development of the TR sequence and meter-scale cycles is driven by glacio-eustacy where the main sequence is 4^{th} order (~400 Ky) with superimposed meter-scale cycles that are 5^{th} and/or 6^{th} order (~100 Ky). Nevertheless, erosional capping surfaces within the more proximal tempestites represent ancient rocky shorelines that developed during forced sea level falls. In order to explain this stratigraphic architecture, a carbonate open-ramp model is proposed with a concave-up profile and a narrow and steep inner ramp in equilibrium with a high-energy coastline.

Acknowledgements

I would like to express how grateful I am to my appreciated supervisor André Desrochers for his adaptation and patience, his guidance throughout the project, his financial support and his generosity. I particularly appreciated his style of allowing his students to adapt themselves to a new study and research environment.

Many thanks go also to R.W.C. Arnott for his comments, as well as Simone Dumas for her expertise. Pierre Bertrand merits heartfelt acknowledgements for his help drafting and correcting the figures, several times.

I would like to thank my colleague and friend Atul Kulkarni (M.Sc. candidate) for his critical point of view. And most importantly, I would like to give special thanks to my family for their support and to my life partner, Marie-Catherine Drigeard Desgarnier, for her constant encouragements.

Table of Content

List of Tables

List of Figures

1 - Introduction

The Llandovery of Anticosti Island, Québec is one of the thickest shallow water carbonate sections in North America. It is of particular interest because of its continuous, extremely fossiliferous and largely undisturbed succession of shallow marine deposits. The Jupiter and Chicotte formations were extensively studied for their faunal richness (Copper, 1981, 1997; Brunton, 1988; Barnes, 1989; Brunton and Copper, 1994; Copper and Jin, 1995; Copper and Long, 1998; Jin and Copper, 1998, 2000; Dewing, 1999; Jin, 2008; Ausich and Copper, 2010; Nestor et al., 2010) but little for their sedimentology and stratigraphic architecture (Brunton and Copper, 1994; Copper and Long, 1990; Desrochers, 2006).

Limestones and siliciclastics, across the Jupiter-Chicotte formational contact, allow me to study the sediment dynamics on a storm-dominated, carbonate ramp that was slowly subsiding while a glacial episode was causing high-frequency sea level oscillations. Furthermore, understanding the stratigraphic architecture remains a delicate task, as internal erosional surfaces are common within the Chicotte Formation without obvious evidence of either intertidal sedimentation or subaerial exposure (Desrochers, 2006). This study focuses on the following objectives: 1) to present a description of facies across the Jupiter-Chicotte formational boundary, 2) to correlate these along the four studied sections based on sequence stratigraphy, 3) to explain the sudden domination of crinoids in the Chicotte Formation, 4) to understand the regional and global driving mechanisms of the sediment dynamics including spatial and temporal variation in siliciclastic content, and 5) to propose a suitable depositional model.

1.1 - Geological Setting

Anticosti Island is located at the entrance of the Gulf of St. Lawrence about 30 km south of the Quebec North Shore and 75 km northeast of the Gaspe Peninsula (Fig. 1). The island is 222 km long and 56 km wide. A thick mixed carbonate-siliciclastic section (~900 m) is exposed on Anticosti and represents one of the most complete successions spanning the Ordovician/Silurian (O/S) boundary (Barnes, 1989; Long, 2007). Above the Upper Ordovician strata, the Anticosti section includes a nearly complete Llandovery succession (up to 400 m) representing sediments accumulating in a storm-influenced, mid to outer carbonate ramp typically, except for some shallow-water reefal and shoreface deposits (Brunton and Copper, 1994; Desrochers, 2006; Long, 2007). Geological mapping of Anticosti Island changed drastically from the original map (Twenhofel, 1928)

Figure 1: Location of Anticosti Island and study area. The oldest Formation (Vauréal) is in the North whereas the youngest (Chicotte) in the South. The four visited locations are respectively: Pointe au Cormoran (1), Bell River (2), Pointe Sud (3) and Pointe Sud-Ouest (4).

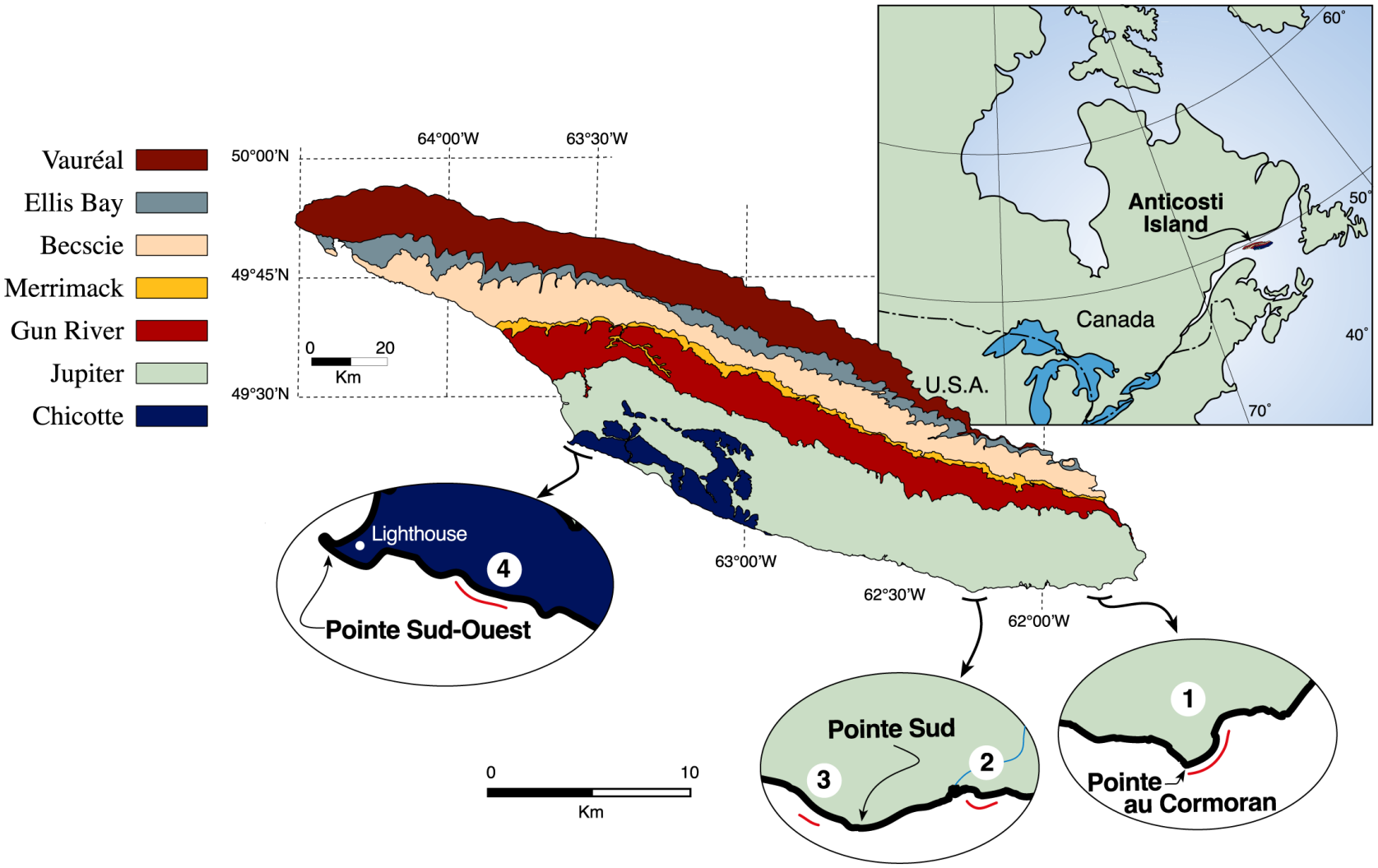
Vauréal
Ellis Bay
Becscie
Merrimack
Gun River
Jupiter
Chicotte
50°00'N
49°45'N
49°30'N
64°00'W
63°30'W
63°00'W
62°30'W
62°00'W
0
20
Km
0
10
Km
Anticosti Island
Canada
U.S.A.
60°
50°
40°
70°
Lighthouse
4
Pointe Sud-Ouest
Pointe Sud
3
2
1
Pointe au Cormoran

to the most recent one (Desrochers and Gauthier, 2009) because inland mapping is now greatly facilitated by several primary and secondary access roads (Fig.1).

During the Early Silurian, the Anticosti Basin, located along the northwestern margin of the Iapetus Ocean (Scotese, 1997), was at paleolatitudes of 15° to 20° south within the peri-equatorial, hurricane-affected belt (Nestor et al., 2010). At that time, Laurentia was partly covered by shallow epeiric seas (Nance and Linnemann, 2008). At a more global scale, direct evidence has been found for several glaciation pulses throughout the Llandovery; including tillite deposits, glacially-faceted and striated clasts, and glaciomarine gravity flow deposits largely present in South America (Grahn and Caputo, 1992; Diaz-Martinez and Grahn, 2007). In addition, sea-level lowstands and glacial tillite deposits in the Amazon Basin and Africa coincide with positive $\delta^{18}O$ excursions suggesting important global climatic and eustatic changes during the Llandovery (Azmy et al., 1998).

The O/S Anticosti section was part of a foreland basin that developed initially during the partial closure of Iapetus Ocean at the onset of the Taconic orogeny (Lavoie, 2008). The sediments accumulated in this long term subsiding basin under the influence of Taconic and post-Taconic load that allowed preservation of a nearly complete record of sedimentation, especially during the more tectonically quiet Early Silurian interval (Long, 2007, Desrochers et al., 2010). The Anticosti succession should provide therefore, a sensitive indicator of subtle climatic and eustatic changes throughout this time interval.

The Anticosti succession (Fig. 2) is largely unaffected by tectonic stress with well preserved sub-horizontal strata (Petryk 1981; Copper and Long 1998). Petryk (1981) noted, however, that local faults are mostly normal, with high dips and meter-scale relative displacement; folds are broad and fold axes are mostly parallel to stratigraphic dip. Four sets of fractures were later identified and related to the early Acadian to Jurassic tectonic events (Bordet et al., 2010). In addition, most of the surface lineament directions are related to the fracture sets (Bordet et al., 2010). Bordet et al. (2010) observed some open folds oriented WSW-ENE at Pointe du Sud-Ouest, which are well imaged on offshore seismic profiles between Anticosti and Gaspé Peninsula (SOQUIP, 1987). These open folds formed during the Middle Devonian Acadian orogeny.

Figure 2: Tectonic context and stratigraphy of the Anticosti succession. The first section (left) presents the tectonic context of the Anticosti Basin and structures development on Anticosti Island (after Bordet et al., 2010). Generalized stratigraphic sections of the Anticosti succession (center) and of our studied interval (right) across the Jupiter-Chicotte formational boundary are illustrated. The Telychian time slices, *Te1* and *Te2*, follow the use of Cramer et al. (2011) and Munnecke and Männik (2009).

Time
Jurassic
Major tectonic events
Orogenies
Rifting
Atlantic Ocean
Structures development on Anticosti Island
Fractures
Folds
Faults
Dikes
Sedimentation Erosion
Sedimentation
Burial
Erosion
Ordovician
Silurian
Devonian
Early
Middle
Late
Taconian
Early Acadian
Acadian
Inferred
Development
Possible reactivation
Periods
Series
Stages
Upper Ordovician
Lower Silurian
Ashgill
Landovery
Hirnan-tian
Rhuddanian
Aeronian
Telychian
Te 1
Te 2
Rawtheyan
Merrimack
Formations
Vaureal
Ellis Bay
Becscie
Gun River
Jupiter
Chicotte
General section
100 m
2 m
Members
Pavillon
Brisante
Calcareous shale with calcarenite
Argillaceous limestone
Sandstone with limestone lenses
Calcareous shale
Limestone with shale interbedded
Encrinitic limestone
Limestone
Coral-stromatoporoid bioherm

1.2 - Jupiter and Chicotte Formations: Previous Work

The Jupiter and Chicotte formations (Fig. 2) are the uppermost units exposed on Anticosti Island (Copper, 1981; Petryk, 1981). The first description of these formations was by Richardson in his Report of the year 1857. He named Formation E, the actual Jupiter Formation, although he was unable to measure a complete succession, he estimated its thickness to be 171m, which is remarkably accurate when compared to more recent studies: 200 m in Twenhofel (1928), 145 m in Bolton (1972), 171 m in (Petryk 1981), 167 m in Copper and Long (1990) and 164-168 m in (Long 2007). Petryk was the first to use a helicopter to access the different exposures before roads were built on the south central and southeastern parts of the island in the 1980's. The Chicotte Formation was described in Twenhofel (1928), Bolton (1972) and Petryk (1981) who estimated its thickness to 22 m, 23-33 m and less than 75 m respectively. More recent roads, however, provided critical access to new outcrops of the Chicotte Formation. Petryk (1981) was the only one approaching the current estimated thickness: more than 90 m in Brunton and Copper (1994), ~90 m in Long and Copper (1994) and ~80 m (Desrochers, 2006).

The Jupiter Formation consists of calcareous mudstone, micrite, grainstone and minor intraformational conglomerate (Long, 2007). It marks the highest diversity of shelly communities (over 100 brachiopod species) in the entire Anticosti succession (Copper and Jin, 1995), and notably including shellbeds (Copper, 1997). Copper and Long (1990) divided the formation into six members: Goéland, East Point, Richardson, Cybèle, Ferrum, and Pavillon. The Pavillon Member, which is overlain by the Chicotte Formation, comprises 10-12 m of recessive calcareous mudstone and interbedded micrite, with discontinuous lenses of calcarenite containing broken brachiopods and abundant crinoid ossicles (Long and Copper, 1994). It is a part of a shallowing upward package (from the Jupiter Cybèle Member to the Chicotte Formation) deposited in a shallow subtidal, storm influenced setting (Desrochers, 2006). It has the most diverse fauna of brachiopods and corals found in the Jupiter members. The coral and stromatoporoid fauna is similar to that of the overlying Chicotte Formation, but much less diverse (Copper and Long, 1990).

The Chicotte Formation is dominated by encrinites (limestone with over 50% crinoids bioclasts as defined by Ausich (1997)) that represent a proximal mid-ramp sand-shoal complex (Brunton and Copper, 1994; Desrochers, 2006). This complex (at least 80 m thick) prograded over the more distal mid- to outer- ramp facies of the underlying Jupiter Formation in response to a long-term sea level fall during early Telychian time (Desrochers, 2006). Reefal limestones (frame- bind-

and bafflestone) including mud-rich fenestrate bryozoans-sponge (Desrochers et al., 2007) and coral-stromatoporoid (Brunton and Copper, 1994) buildups are also present. Brunton (1988) described two major reef complexes (10-20 m and 50-80 m above the formation base) with bioherms up to 100 m in diameter, and localized biostromes and patch reefs near the base. The typical depositional unit in the Chicotte Formation is a metre-scale, shallowing-upward subtidal cycle indicating higher frequency sea-level changes (Desrochers, 2004). Desrochers (2006) described intraformational high-relief erosional surfaces within the Chicotte Formation interpreted as Telychian rocky shores.

The distinct lithological change at the Jupiter-Chicotte boundary, first identified by Schuchert and Twenhofel (1910) and later re-examined by Bolton (1972), and Brunton (1988), displays recessive limestones interbedded with shale overlain abruptly by resistant encrinites units at the Jumpers Cliff. Jin and Copper (1998) mapped some Chicotte outcrops near South Point, but did not document any outcrop showing its contact with the underlying Jupiter Formation.

The Jupiter and Chicotte formations are Aeronian and Telychian in age (Barnes, 1989; Copper and Long, 1990). Distribution of conodonts and geochemical data, correlated with the Viki Core in Estonia, suggest an Early Telychian age for at least the lower half of the Chicotte Formation (Munnecke and Männik 2009). Using the *Silurian Chronostratigraphic Chart* from Cramer et al. (2011), the Jupiter-Chicotte boundary is at the *Te1*/*Te2* time slice boundary implying an Early Telychian age also for the uppermost Jupiter members. Based on brachiopod and conodont data, Copper and Long (1990) draw some correlations with the Llandovery Series of the type area in the U.K.: they affirmed that the Pavillon Member is of C5 age (*Icriodella inconstans* Zone – Mid Telychian) and consistent with their data, but they thought this correlates only with the lower part of the C5 strata in the U.K. (using *Eocoelia curtisi* as a key species). The upper age limit of the Chicotte Formation remains unknown.

The Pavillon Member of the Jupiter Formation marks a shift in fauna (Nestor et al., 2010) accompanied by a positive stable isotope $\delta^{13}C$ excursion (Munnecke and Männik, 2009). The Pavillon fauna predicts, in many aspects, the succeeding Chicotte fauna, marking a strong surge in stromatoporoid diversity and abundance (Nestor et al., 2010). As noted in some early work (i.e. Twenhofel, 1928), the Chicotte is the only formation on Anticosti Island in which the number of crinoids, coral and stromatoporoid species outnumber the brachiopod shelly benthos with the exception of reefal units such as the East Point Member in the underlying Jupiter Formation (Copper and Long, 1990). Crinoid richness doubled from Aeronian to Telychian age (Ausich and Copper, 2010). Furthermore, many new species appeared at the base of the Chicotte Formation (Ausich and

Copper, 2010, their Fig. 4). An important shift is also noted in the brachiopod communities (Copper and Jin, 1995, their Fig. 4) with a reduction in diversity of pentamerids (Jin and Copper, 2000) and strophomenids (Dewing, 1999) at the top of the Jupiter Formation.

1.3 - Methodology

Data for this research were provided by fieldwork and laboratory techniques through different approaches: section description in the field, petrography observations, and mineralogical and geochemical analyses in the laboratory.

Four sections were measured along superbly exposed coastal outcrops at the east, south and southwest ends of the island. Easternmost and westernmost sections are 150 km apart (Fig. 1). Sections have been described bed by bed using standard tools as sedimentology and stratigraphy integrated with the modern approach of cyclostratigraphy and sequence stratigraphy.

The easternmost section (Fig. 1) was described on the east side of Pointe au Cormoran (Section 1: UTM 20U 0586525-54360059). It comprises 8.5 m of the Pavillon Member and 2 m of the basal Chicotte Formation (Fig. 3). Twenty-two (22) rock samples selected for thin sections and one shale (FC-3) were collected at this location.

Two sections were measured near the South Point (Fig. 1), one about 500 m east of the Bell River mouth (Section 2: UTM 20U 0558552-5435718) and the other on the west side, about 4.5 km from the Bell River mouth (Section 3: UTM 20U 0553533-5435243). The possible presence of exposed Chicotte strata at these two locations is still hypothetical, for now we will assume that both sections are within the uppermost Jupiter Formation close to its upper boundary. Section 2 (Fig. 4) shows 9.5 m whereas Section 3 (Fig. 5) shows 3.5 m within the Pavillon Member. Twenty (20) and 12 rock samples for thin sections were respectively taken at sections 2 and 3. Shale (FC-4) was also sampled at Section 3.

The westernmost section was measured east of the Anse Gibbons (Fig. 1), about 4 km east of the Southwest Point (Section 4: UTM 20U 0461091-5469995). It covers 8 m of the uppermost Jupiter Formation and 6 m of the basal Chicotte Formation (Fig. 6). It is the only location providing a good description of the Jupiter and Chicotte boundary (Copper and Long, 1990). A total of 31 samples were collected at Section 4; two (2) shales (FC-5 and 6) and 29 carbonates for thin sections.

Thin section samples were chosen at regular intervals according to changes in lithology. Each thin section was stained with a solution of Alizarin Red S and Potassium Ferricyanide. This

Figure 3: Detailed stratigraphical log of Section 1, Pointe au Cormoran, showing stratigraphic position, facies number, lithological characteristics, and sequence stratigraphic interpretation. Note that the presence of the Chicotte Formation at the top of this section will be discussed in section 7.1.

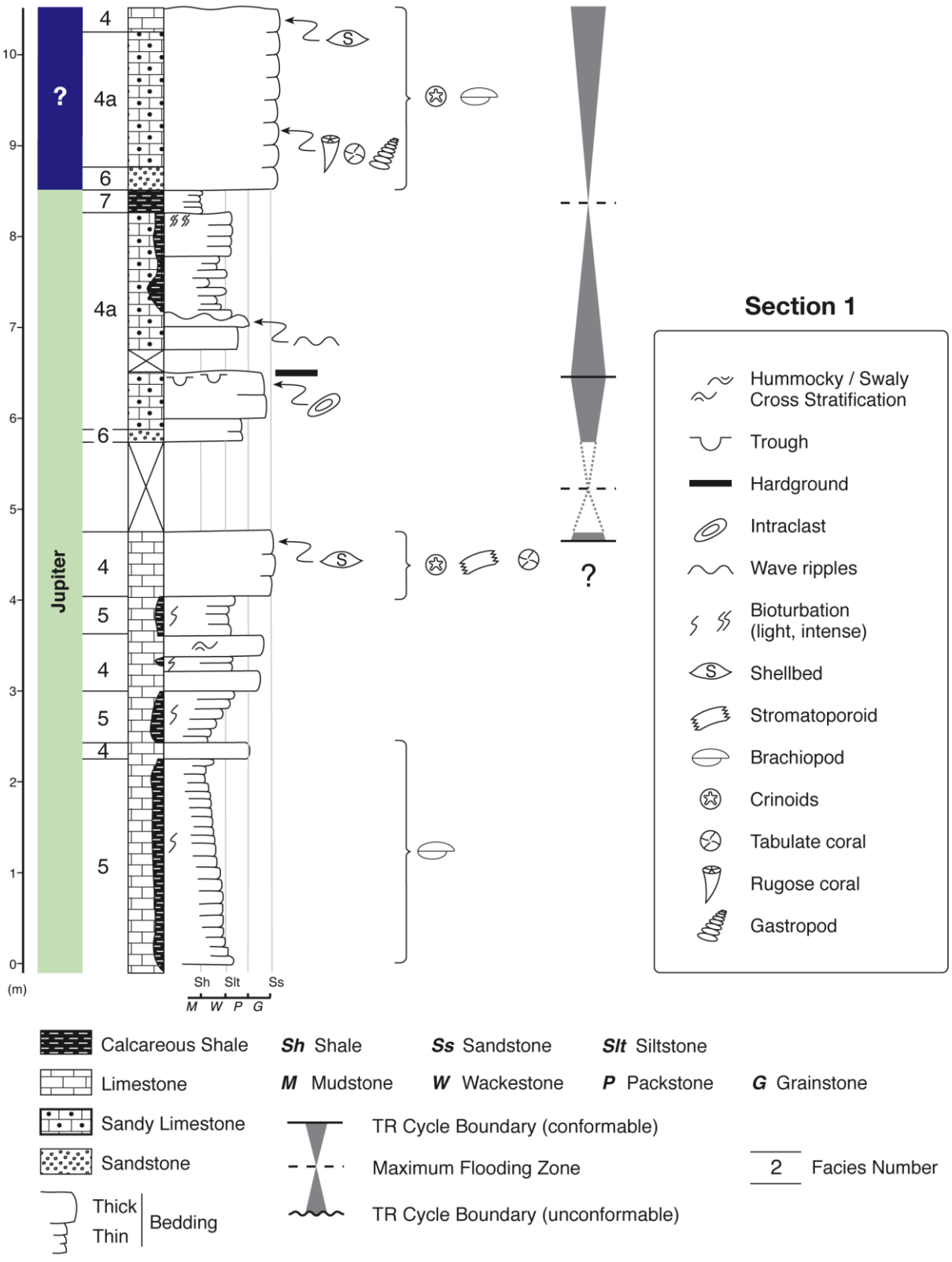
Section 1
Jupiter
?
4
4a
6
7
4a
6
4
5
4
5
4
5
S
S
?
Sh
Slt
Ss
M W P G
(m)
0
1
2
3
4
5
6
7
8
9
10
Hummocky / Swaly Cross Stratification
Trough
Hardground
Intraclast
Wave ripples
Bioturbation (light, intense)
Shellbed
Stromatoporoid
Brachiopod
Crinoids
Tabulate coral
Rugose coral
Gastropod
Calcareous Shale
Limestone
Sandy Limestone
Sandstone
Thick
Thin
Bedding
Sh Shale
Ss Sandstone
Slt Siltstone
M Mudstone
W Wackestone
P Packstone
G Grainstone
TR Cycle Boundary (conformable)
Maximum Flooding Zone
TR Cycle Boundary (unconformable)
2
Facies Number

staining allows us to differentiate most common carbonates minerals as calcite and dolomite and their relative iron content (Dickson, 1966). Thin sections were described in order to complement observations made in the field.

In total, six (6) shale samples were taken, from which two (2) for comparative analysis: one from the Ellis Bay Formation (Hirnantian age; FC-1) and one from the Merrimack Formation (Rhuddanian age; FC-2). Each sample was heated at 60°C for four (4) hours to dry and then ground to obtain a clay grain size (< 2 μm). Samples were then analyzed by standard X-ray fluorescence (XRF) and X-ray diffraction (XRD) (Tucker, 1988).

1.4 - Terminology

Carbonates are described using Dunham (modified by Embry and Klovan, 1971) and Grabau classifications. “Calcareous shale” designates any very fine (clay- to silt- sized), recessive-weathering, commonly fissile sediment composed by a mixture of siliciclastic and carbonate material in varying proportions. The use of the “/” symbol between two lithologies indicates that the designated object is characterized by a continuum between these two lithologies. For example, “mudstone/wackestone” means that beds of mudstone and wackestone are present. In the present study, the carbonate ramp profile is divided into inner, mid-, and outer ramp with a proximal-distal gradient within the mid-ramp (see below Fig. 7). Fair weather wave base (FWWB) coincides with the base of the inner ramp and storm wave base (SWB) with the base of the mid-ramp. This carbonate ramp is storm-dominated and is in equilibrium with a high energy coastline (see section 7.3). Along this storm-dominated ramp, proximal to distal tempestites are deposited on the proximal to distal mid-ramp/outer ramp. A continuum of processes are involved in the deposition of sediments from high energy, erosive and episodic combined flows to waning flows to wave-enhanced sediment-gravity flows. Combined flows present two components: wave-induced oscillatory flows effectively throwing sediment into suspension, and a unidirectional geostrophic flow able to carry sediment down-current. Waning flows present the same characteristics as combined flows but the unidirectional component is weakening as the storm wanes. Finally, wave-enhanced sediment-gravity flows, present only wave induced oscillatory flows allowing sediment in suspension to progress down ramp along a density gradient (see Section 4 for details).

2 - Section Description

The individual sections are composite and extend for a few hundreds of meters along the coast. They are all near the Jupiter and Chicotte formational contact. Outcrop exposures are exceptional, especially along the southern island shoreline. Geological units are slightly dipping to the south (~1°) allowing coastal outcrops not to form vertically extensive cliffs, but more accessible sections. Beds are lenticular in shape with limited lateral extension eroding into the background lithology or into each other. Horizons are difficult to correlate at the bed scale even just a few tens of meters apart.

Section 1 is here described for the first time and characterized by a lower carbonate-dominated unit with minor siliciclastic component (Fig. 3, Plate 1A). Above a meter thick covered interval, a second unit composed of mixed siliciclastics and carbonate with some distinct sandstone and shale beds crops out (Plate 1B). Facies are dominated by more or less sandy bioclastic grainstone/packstone/rudstone and HCS sandstone.

Several sedimentary structures are common including hummocky cross-stratification (HCS), uni- or bi-directional large wave ripples (LWR), south oriented trough cross beds and hardgrounds (see section 4.7). Taphonomic features are also present: massive reworked corals, transported benthic fauna, clasts perforation and intensely bioturbated beds. An anomalous abundance of solitary rugose corals, associated with transported tabulate corals and gastropods is present around 9.5 m above the base of the section.

Section 2 has been described by Copper and Long (1990) and sampled for brachiopods by Jin and Copper (2000). The whole section is carbonate-dominated with some minor shale interbeds (Fig. 4). Siliciclastic material increases upward. In the lower part, facies are dominated by bioclastic grainstone/packstone, calcarenites/calcirudites eroding into bioturbated mudstone/ wackestone. Progressively, this mudstone/wackestone is replaced upward by shale (Plate 1D).

LWR are present at the base of the section (Plate 1C). Diversified fauna are common with some prominent brachiopods shell beds (see section 4.3) around 2.5m and 4.5m, above the base of the section, as recognized by Copper and Long, 1990. Bioturbation is abundant in the first three meters. Fauna is rarely *in situ*, rugose corals are overturned and brachiopods disarticulated.

Figure 4: Detailed stratigraphical log of Section 2, Bell River, showing stratigraphic position, facies number, lithological characteristics, and sequence stratigraphic interpretation.

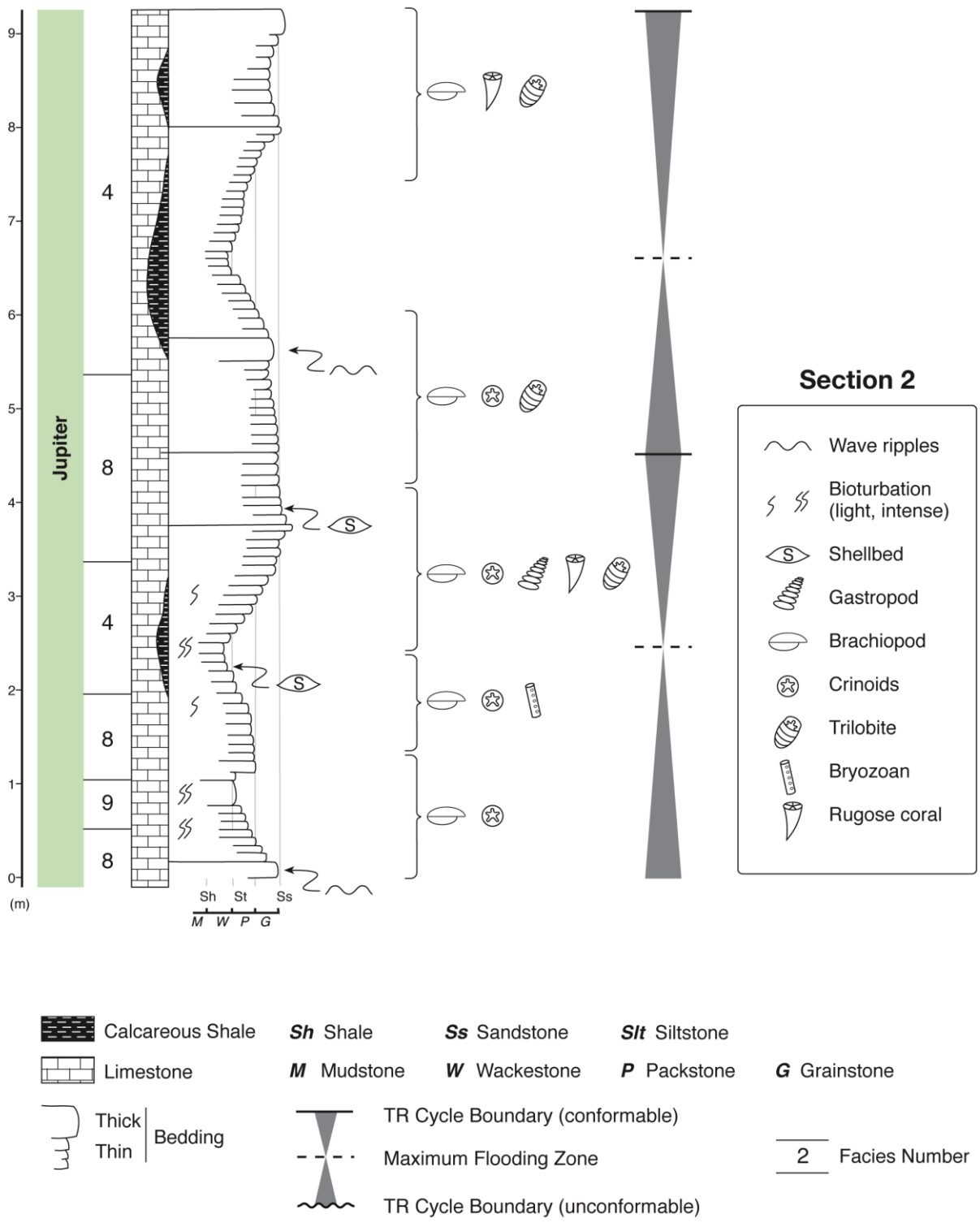
Jupiter
(m)
Sh St Ss
M W P G
Section 2
Wave ripples
Bioturbation (light, intense)
Shellbed
Gastropod
Brachiopod
Crinoids
Trilobite
Bryozoan
Rugose coral
Calcareous Shale
Limestone
Thick
Thin
Bedding
Sh Shale
Ss Sandstone
Slt Siltstone
M Mudstone
W Wackestone
P Packstone
G Grainstone
TR Cycle Boundary (conformable)
Maximum Flooding Zone
TR Cycle Boundary (unconformable)
2 Facies Number

Figure 5: Detailed stratigraphical log of Section 3, South Point, showing stratigraphic position, facies number, lithological characteristics, and sequence stratigraphic interpretation. Note that the presence of Chicotte Formation at the top of this section will be discussed in section 7.1.

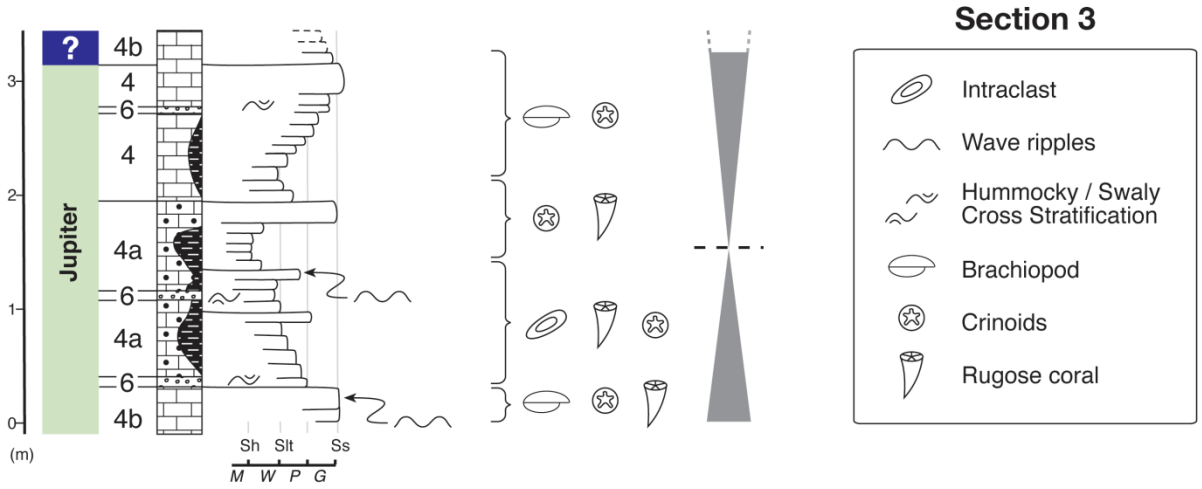
Section 3
Jupiter
?
4b
4
6
4
4a
6
4a
6
4b
3
2
1
0
(m)
Sh Slt Ss
M W P G
Intraclast
Wave ripples
Hummocky / Swaly Cross Stratification
Brachiopod
Crinoids
Rugose coral
Calcareous Shale
Limestone
Sandy Limestone
Sandstone
Thick
Thin
Bedding
Sh Shale
Ss Sandstone
Slt Siltstone
M Mudstone
W Wackestone
P Packstone
G Grainstone
TR Cycle Boundary (conformable)
Maximum Flooding Zone
TR Cycle Boundary (unconformable)
2
Facies Number

Figure 6: Detailed stratigraphical log of Section 4, east of the Anse Gibbons, showing stratigraphic position, facies number, lithological characteristics, and sequence stratigraphic interpretation.

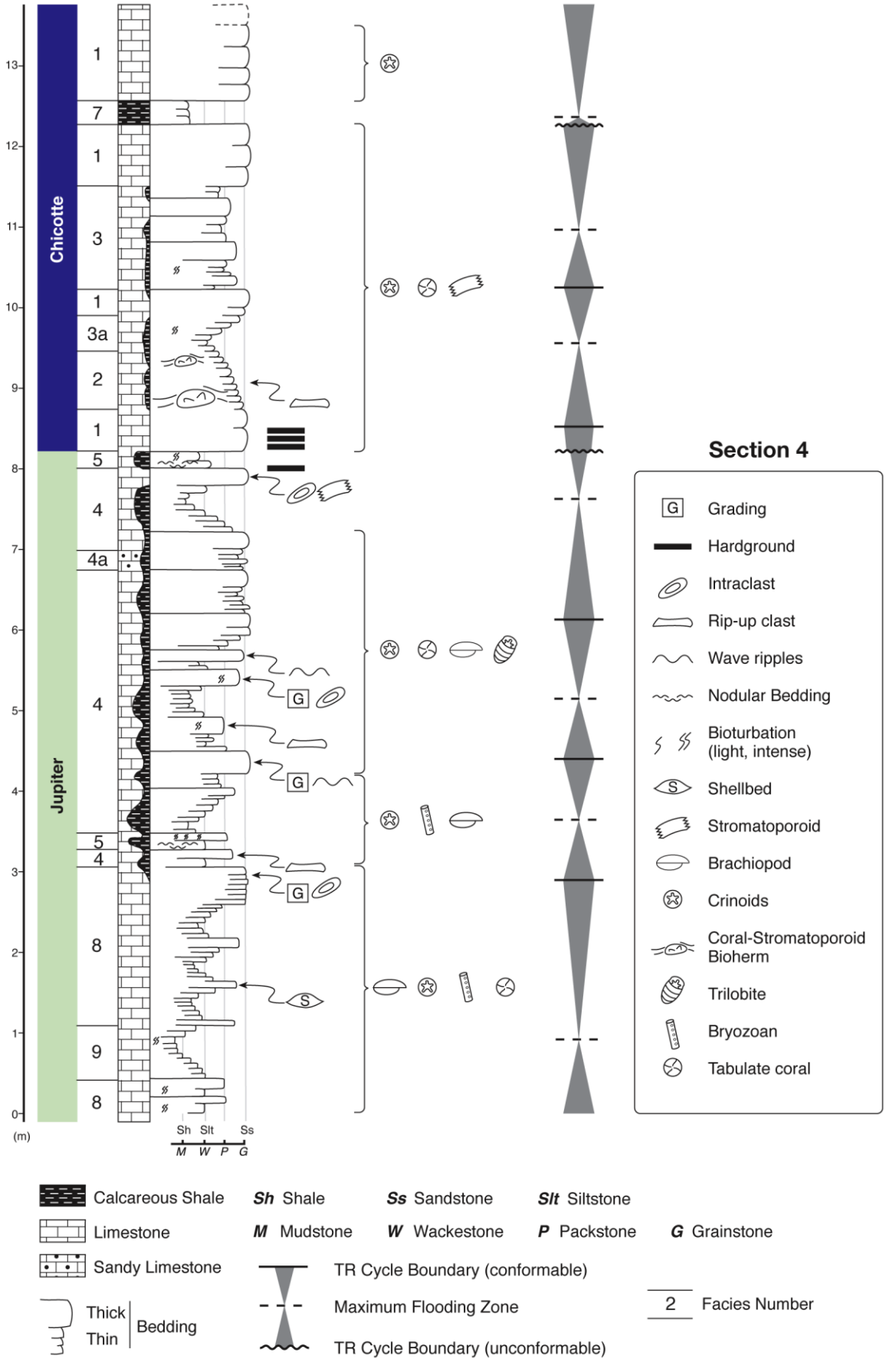
Chicotte
Jupiter
Section 4
Grading
Hardground
Intraclast
Rip-up clast
Wave ripples
Nodular Bedding
Bioturbation (light, intense)
Shellbed
Stromatoporoid
Brachiopod
Crinoids
Coral-Stromatoporoid Bioherm
Trilobite
Bryozoan
Tabulate coral
(m)
Sh Slt Ss
M W P G
Calcareous Shale
Limestone
Sandy Limestone
Thick
Thin
Bedding
Sh Shale
Ss Sandstone
Slt Siltstone
M Mudstone
W Wackestone
P Packstone
G Grainstone
TR Cycle Boundary (conformable)
Maximum Flooding Zone
TR Cycle Boundary (unconformable)
2 Facies Number

Section 3 is known as a sampling locality for pentamerid brachiopods (e.g. Jin and Copper, 2000; Jin, 2008). It consists of more than three meters of mixed siliciclastic-carbonate deposits (Fig. 5). The base of the section is characterised by a LWR bed. Facies are thinly alternating between bioclastic packstone/grainstone, sandy packstone/grainstone, sandstone and shale (Plate 1E).

Several sedimentary structures are common such as HCS, very fine laminations in sandstones, and uni- or bi-directional LWR in two different beds (see section 4.5). Abundant solitary rugose corals in some horizons are also present.

Section 4 (Fig. 6), first described as the Jumpers section by Richardson (1857), was also visited by Twenhofel (1928), Petryk (1981), Copper and Long (1990). It is a classic locality that has been intensively studied for conodonts (Uyeno and Barnes, 1981), stromatoporoid biostromes/bioherms (Brunton, 1988; Brunton and Copper, 1994) and brachiopods (Dewing, 1999, Jin and Copper, 2000). Section 4 exposes more than 13 meters (Fig. 6) and is subdivided into three packages: lower, mid and upper (Plate 1G). The lower package (0 to 3 m above the section base) is carbonate dominated. It consists of lenticular bioclastic packstone/grainstone/rudstone beds, within bioturbated mudstone/wackestone. The middle unit (3 to 8 m above the section base) is characterized by an alternation of bioclastic packstone/grainstone/rudstone and shale. The upper unit corresponding to basal Chicotte strata shows an alternation of encrinite, minor shale interbeds and coral-stromatoporoid biostromes/bioherms (Plate 1H). The Jupiter-Chicotte boundary is well expressed by the weathering profile (Plate 1F). About two (2) meters above this contact, coral-stromatoporoid biostromes/bioherms are well exposed and also studied by Brunton (1988).

Interesting sedimentary features include LWR, rip-up and intraclasts, intensively bioturbated horizons, preferential crinoidal stem orientation, and erosional surfaces (see chapter 4). We were able to recognize diverse fauna, orbituration beds, shellbeds, massive tabulate coral colonies, biostromes/bioherms and a clear shift in the faunal assemblage at the boundary.

3 - Facies Description

Facies near the Jupiter-Chicotte boundary are differentiated on the basis of their field characteristics: lithology, primary sedimentary structures, trace fossils and other features. Nine (9) facies are present grouped into three (3) distinct facies associations (Table 1; see Section 5). Facies description is not only a genetic approach but mainly based on observations in order to group them after in the facies assemblages to better understand the depositional environment (see Section 5).

Plate 1: Field photographs showing studied sections at different localities. JU = Jupiter, CH = Chicotte. Red dashed line separates different formations (or members). White or black dashed lines separate different facies. Red arrows point out specific features. See Chapter 3 for facies description. **A)** Field photograph of the lower carbonate unit in lower part of Section 1. Note the alternation of more resistant, lighter crinoid rich facies (4) and more recessive, darker brachiopod rich intervals (Facies 5) showing a coarsening upward trend. Scale in decimeters (1 m): meter. **B)** Field photograph of uppermost Jupiter beds in the upper part of Section 1. Note the variable amount of fine material in Facies 4a. Scale in decimeters (1 m): meter. **C)** Field photograph of the base of Section 2 exposing the basal bed with symmetrical dune structures on a plane bed. Red arrows point two different dune crests indicating their orientation. Scale in meters: person. **D)** Field photograph of upper Section 2 (approximately 4 to 9 meters above the base). Facies boundary is clearly visible here due to the change in color probably related to siliciclastic supply (darker is more shally). Scale in meters: person (circled). **E)** Field photograph of an almost complete view of Section 3. Note the fine alternation of siliciclastic and carbonate beds only a few kilometers westward from Section 2. Scale in decimeters (1 m): meter. **F)** Field photograph of the overhang at Section 4 representing the possible Jupiter and Chicotte formational boundary (8 meters above the section base). Scale in meter (1 m): scale bar. **G)** Field photograph of Section 4 showing a lower carbonate dominated unit, a middle unit characterized by bioclastic calcarenites-calcirudites with shale interbeds and an upper unit starting with the first Chicotte encrinites with minor shale (3 to 9 m above the section base). Note the difference in texture in these three units: a lower massive carbonate unit with subtabular beds, a middle recessive siliciclastic-carbonate unit with subtabular to lenticular limestone beds and shale interbeds, and an upper massive encrinitic unit. Scale in meters: person holding a meter-long staff. **H)** Field photograph of the basal Chicotte Formation in Section 4 (approximately from 8.5 to 11 m above the section base). Note the presence of a small massive coral-stromatoporoid bioherms within encrinitic limestones. Scale in decimeters (1 m): meter.

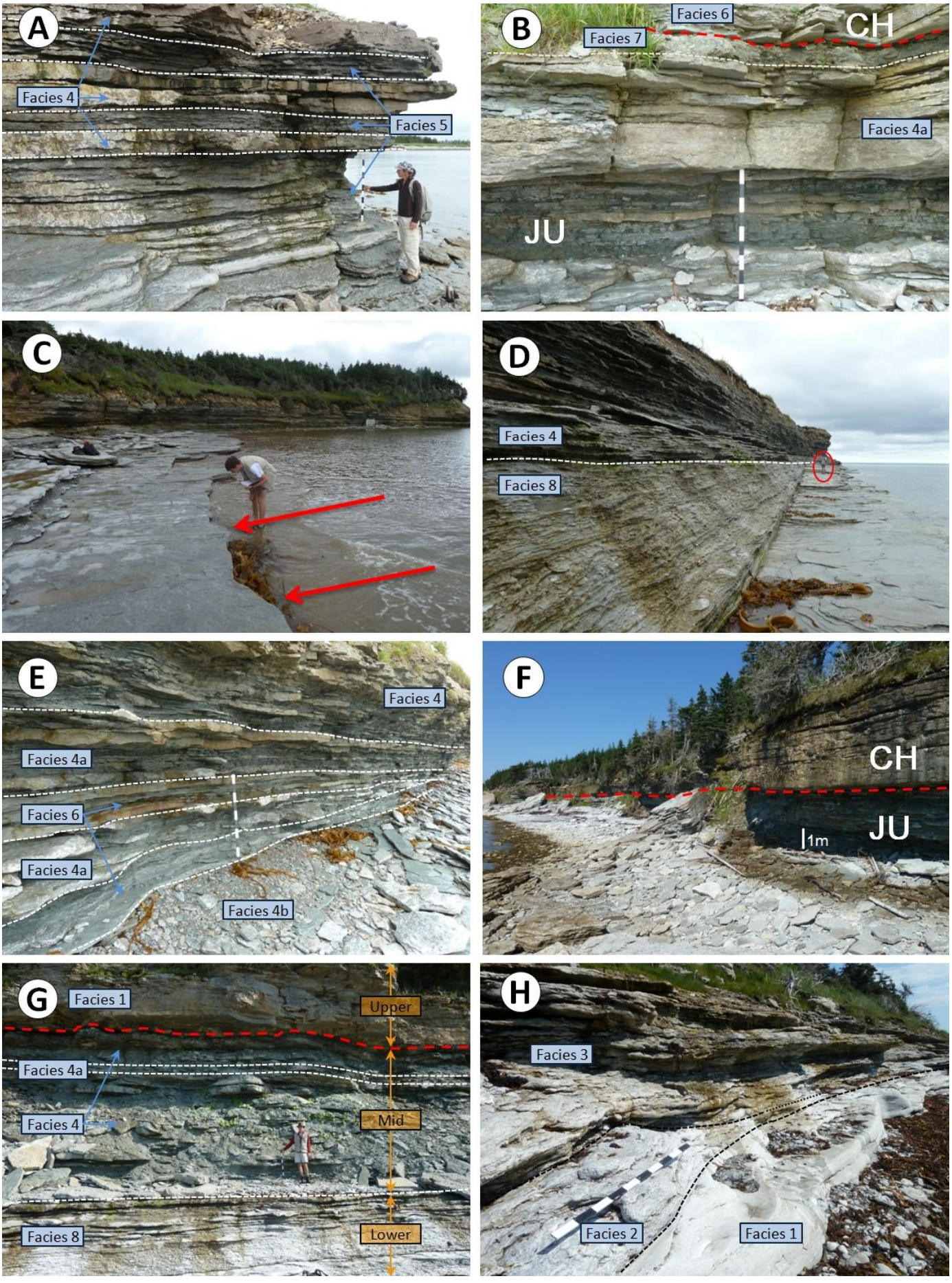
A
Facies 4
Facies 5
B
Facies 6
Facies 7
CH
Facies 4a
JU
C
D
Facies 4
Facies 8
E
Facies 4
Facies 4a
Facies 6
Facies 4a
Facies 4b
F
CH
1m
JU
G
Facies 1
Upper
Facies 4a
Facies 4
Mid
Facies 8
Lower
H
Facies 3
Facies 2
Facies 1

Based on microscopic attributes, three (3) additional microfacies are recognized according to the relative abundance of unusual skeletal or non-skeletal grains (e.g. calcareous algae, calcimicrobe…). For each facies, a description and a brief interpretation of its depositional environment is first provided. Associated sedimentary structures are then described and interpreted.

A detailed and systematic survey of the faunal elements present in our sections is beyond the scope of this study. Nevertheless, some general observations can be made. In the Pavillon Member of the Jupiter Formation, a relatively diverse fauna dominated by brachiopods is present. Other megafossils include: crinoids, ostracods, bryozoans, trilobites, rugose and tabulate corals, together with mollusks and stromatoporoids. The basal Chicotte strata contain a less diverse fauna dominated largely by crinoids. Only minor taxa are present including brachiopods and bryozoans. A distinct faunal assemblage with diverse tabulate corals and stromatoporoids is, however, locally present in small bioherms (for details, see Brunton, 1988; Brunton and Copper, 1994).

3.1 - Facies 1 – Amalgamated Encrinites

This facies is characterized by medium to thick bedded (10 to 50 cm), amalgamated massive crinoidal packstone/grainstone/rudstone (Plate 2A). Scour surfaces are present at the base of the massive limestones (Plate 3C) and immediately overlain by normally graded crinoid rich sediments. The texture varies from clean, well-washed grainstone/rudstone to finer grained packstone/ grainstone. These encrinites are amalgamated or stacked and lack shale interbeds or partings. Crinoid stems, up to 30 cm long, are common and floating into a finer and disarticulated crinoidal matrix. Encrinites are distinctively light grey in colour (Plate 2A). Several hardgrounds are present in the lowermost Chicotte beds showing locally truncated grains. Only rare brachiopods and bryozoans are found. In thin section, this facies shows a small amount of dolomite selectively replacing the micritic matrix, if present (Plates 3A, 3B and 3C). The uppermost beds of the Chicotte Formation, described in this study, show poorly cemented rocks, probably due to an early alteration of grains prior to cementation (Plate 3A). Calcite cement is dominated by well-developed syntaxial overgrowth with some drusy calcite (Plate 3B). Both calcite cements are largely non-ferroan, but ferroan drusy calcite cement is locally present as the final pore-occluding phase. Poorly developed, cloudy syntaxial overgrowth and drusy calcite cement are present around skeletal grains in the few centimeters below the hardground surfaces.

Individual encrinite beds represent sediment affected by high energy, episodic storm events as evidenced by rapid burial of crinoidal material with a scoured base and internal normal grading.

The general absence of shale interbeds suggests a proximal position on the mid-ramp where fair-weather sediment is not preserved. Hardgrounds represent early marine sea floor (see section 4.7). Similar crinoidal grainstone to packstone have been interpreted as wave and current winnowed crinoidal sand shoals (Spengler and Read, 2010) supporting our interpretation of high energy, episodic storm events.

3.2 - Facies 2 – Coral-Stromatoporoid Boundstone

This facies consists of light grey massive coral-stromatoporoid boundstone (more specifically bindstone) locally forming distinctive sub-meter thick bioherms laterally passing into thinner biostromal unit at the same stratigraphic level (Plate 2A). Individual bioherms are 50 to 80 cm high and 2 to 4 m wide, and spaced every 2 to 10 m. Major reef binders are lamellar stromatoporoids (Plate 2D) and favositid tabulate corals (Plate 2C). Stromatoporoids and Favositids are only a few centimeters thick but can reach up to 60 cm in diameter (Plate 2C). Secondary builders include other tabulate and rugose corals, and bryozoans. The boundstone matrix consists of wackestone/packstone with some calcareous shale partings. This peloid-rich matrix typically shows several phases of sedimentary infilling within larger growth cavities (Plates 3D and 3E). Associated bioclasts are crinoids, calcareous algae, and ostracods (Plate 3E). Biostromes and bioherms flanks and caps consist of bioturbated encrinites interbedded with some minor calcareous shale (see below Facies 3).

Biostromes/bioherms did not reach their diversification stage as evidenced from their simple composition, simple builder growth forms, and their relatively small size (James and Wood, 2010). Thus, these biostromes/bioherms did not evolve further than their colonization stage before giving up in response to a relative sea level rise. There is a general consensus that prolific reef growth is diminished below water depths of 25-30 m, but this was set mainly for modern, photosynthesis dependent coral reefs. Its stratigraphic position between amalgamated encrinites (Facies 1) and encrinites interbedded with calcareous shale (Facies 3) suggests deposition in the proximal mid-ramp; possibly as shallow as 15 to 25 m deep (Brunton, 1988). Similar buildup facies associated with crinoidal grainstone have been identified on a Silurian carbonate ramp (Spengler and Read, 2010) and interpreted as moderate energy mound setting slightly deeper than our Facies 2 reinforcing our interpretation.

Table 1: Description of the facies identified across the Jupiter-Chicotte formational boundary.

	Facies	Composition	Description	Depositional Setting	References
FA-1	Amalgamated encrinites (1)	Packstone/grainstone (100%)	***Packstone/grainstone:*** Medium to thick bedded (10-50cm). Massive. Poorly bioturbated. Amalgamated. Sharp basal contacts and erosional surfaces are common.	Proximal mid-ramp	Spengler and Read, 2010
	Coral-stromatoporoid boundstone (2)	Boundstone (≥90%) Calcareous shale (≤10%)	***Boundstone:*** small bioherms (<1 m high). Major framebuilders are tabulate corals and stromatoporoids. Peloid-rich wackestone/packstone matrix. Interbioherm facies consists of Facies 3 with thin shale interbeds traceable across bioherms cores indicating little synoptic relief above the sea floor during their growth.	Proximal mid-ramp	
	Encrinites interbedded with calcareous shale (3)	Packstone/grainstone (90%) Calcareous shale (10%)	***Packstone/grainstone:*** Thin to thick bedded (5-15cm). Massive. Moderately bioturbated. Mostly amalgamated but also with calcareous shale. Sharp basal contacts are present. ***Calcareous shale:*** Very-thin (0-1cm). Fissile.	Mid-ramp	
	Algal-rich encrinites (3a)	---	***Packstone/grainstone:*** Up to 20 % of skeletal grains of calcimicrobe or calcareous algae.	---	
FA-2	Bioclastic P/G with calcareous shale interbeds (4)	Packstone/grainstone (40-70%) Rudstone (~10%) Calcareous shale (20-50%)	***Packstone/grainstone:*** Thin to thick bedded (5-40cm). Lenticular to subtabular. Discontinuous and sharp based. Locally bioturbated at top. Gutter casts, sharp basal contacts, LWR, and wave-enhanced sediment-gravity flow deposits are present. HCS are rare. ***Calcareous shale:*** Very-thin to thin bedded (1-10cm). Fissile to subnodular.	Distal mid-ramp	Long, 2007; Pérez-López and Pérez-Valera, 2011
	Sandy bioclastic P/G (4a)	---	***Packstone/grainstone:*** Sandy matrix with very fine to fine grained quartz grains. Up to cross laminated grainstone/sandstone.	---	
	Algal-rich bioclastic P/G (4b)	---	***Packstone/grainstone:*** Up to 20% of skeletal grains of calcimicrobe or calcareous algae.	---	
	Nodular bioclastic P/G interbedded with calcareous shale (5)	Packstone/grainstone (40-70%) Calcareous shale (30-60%)	***Packstone/grainstone:*** Thin to medium bedded (5-15cm). Nodular to subtabular. Discontinuous. Locally bioturbated. Sharp basal contacts are present. ***Calcareous shale:*** Very-thin to thin bedded (2-5cm). Fissile.	Distal mid-ramp	
	HCS sandstone interbedded with calcareous shale (6)	Sandstone (~50%) Calcareous shale (~50%)	***Sandstone:*** Very-thin to thin bedded (2-15cm). Very fine to fine grained, angular, HCS cross-stratified micas and quartz grains. Subcontinuous. Locally bioturbated. Sharp basal contacts are present. ***Calcareous shale:*** Very-thin to thin bedded (2-10cm). Fissile to subnodular.	Transition zone / Distal mid-ramp	Long, 2007; Pérez-López and Pérez-Valera, 2011
	Calcareous shale (7)	Calcareous shale (100%)	***Calcareous shale:*** Very-thin to thick bedded (1-30cm). Fissile to subnodular.	Outer ramp to distal mid-ramp	Long, 2007; Spengler and Read, 2010
FA-3	Bioclastic P/G with bioturbated M/W interbeds (8)	Packstone/grainstone (30-60%) Mudstone/wackestone (40-70%)	***Packstone/grainstone:*** Thin to thick bedded (5-40cm). Lenticular. Discontinuous. Sharp based, commonly graded and locally laminated. Locally bioturbated. Wave-enhanced sediment-gravity flow deposits are common. Gutter casts, LWR, and shell beds are present. ***Mudstone/wackestone:*** See below (9).	Distal mid-ramp	Long, 2007; Macquaker, 2010
	Bioturbated M/W (9)	Mudstone/wackestone (100%)	***Mudstone/wackestone:*** Thin bedded (5-10cm). Tabular to subnodular. Continuous. Intensively bioturbated.	Outer ramp to distal mid-ramp	Long, 2007; Pérez-López and Pérez-Valera, 2011

Plate 2: Field photographs of Facies Association 1 (Section 4). All photographs are in cross section view, but C is showing a bedding plane view. Black dashed lines separate different facies. Dotted lines highlight distinct features. **A)** Lower Chicotte strata with the bioherms; 8.5 to 10 meters above the section base. Note the lateral change in thickness between the bioherms core and thinner interbiohermal beds (Facies 2) and the textural difference in adjacent encrinites facies (underlying Facies 1: cleaner and coarser, overlying Facies 3: muddier and bioturbated). Scale: 1 m. **B)** Thin shale parting between encrinites in Facies 3; 8.5 meters above the section base. **C)** Thin lamellar favositid tabulate corals seen from the bottom from a fallen block (Facies 2). 9 meters above the section base. Scale in centimeters (32 cm): hammer. **D)** Closely spaced stromatoporoid colonies showing different growth phases as evidenced by their lateral interrelationships with adjacent sediments. 9 meters above the section base. Scale is a 10 cm ruler.

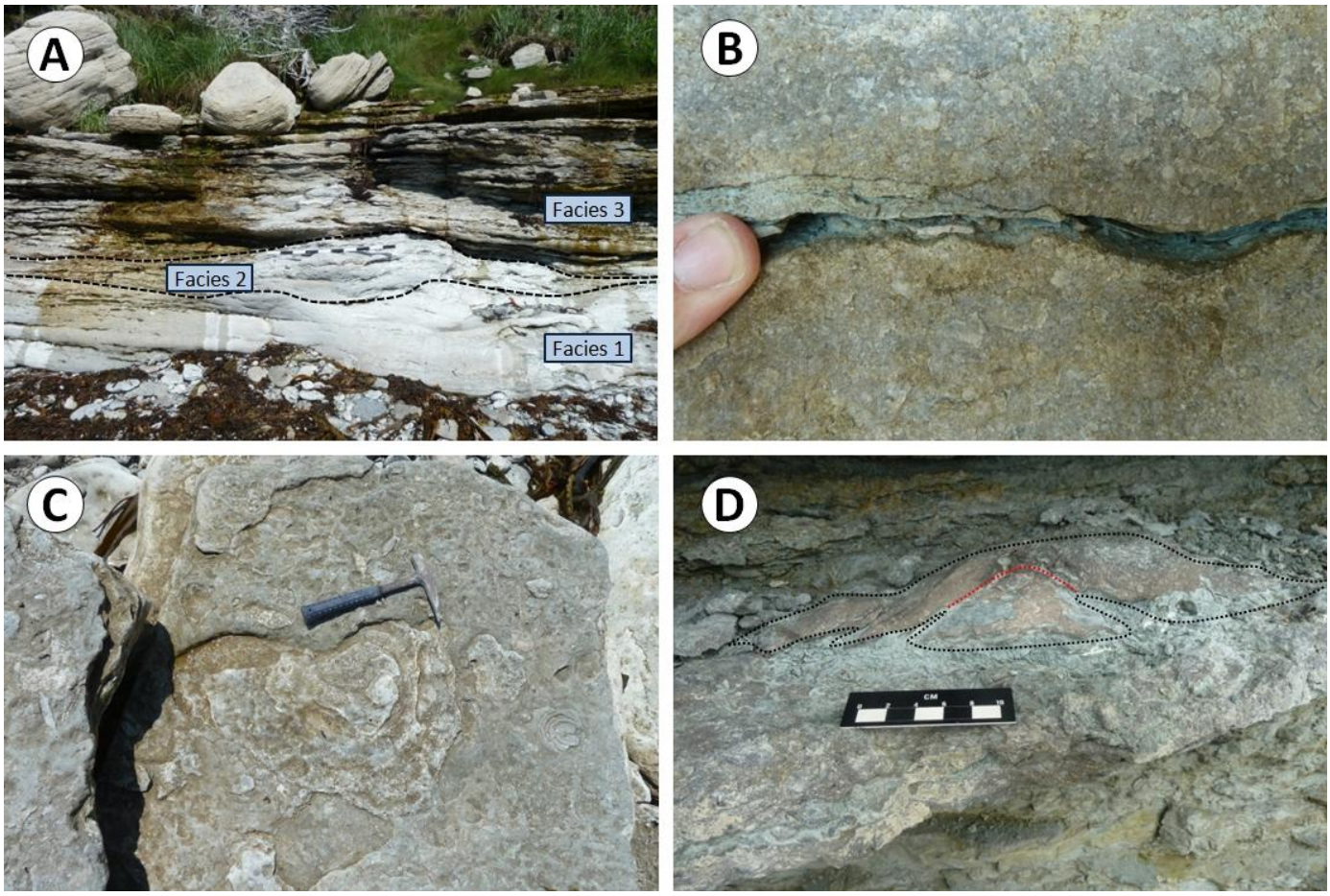
A
Facies 3
Facies 2
Facies 1
B
C
D

Plate 3: Photomicrographs of Facies Association 1 (Section 4). Dotted lines and arrows point out specific features. **A)** Photomicrograph of Facies 1 showing the clean and coarse grained crinoidal fabric. Note the presence of pyrite nucleating around crinoid grains (red arrow) and pre-dating syntaxial calcite cement. 13 m above the section base. Scale bar is 2 mm. **B)** Photomicrograph illustrating clean crinoidal grainstone with syntaxial overgrowth in Facies 1. Ferroan dolomite crystals stained in blue are also present. 11.2 m above the section base. Scale bar is 500 µm. **C)** Photomicrograph showing sharp hardground surface (red dotted line) with a distinct change in crinoidal grain size (Facies 1). Note the presence of blue stained ferroan dolomite crystals and black, opaque crystals of pyrite. 8.5 m above the section base. Scale bar is 5 mm. **D)** Photomicrograph showing the typical boundstone matrix of Facies 2 with a layered (white arrow) peloid-rich wackestone/packstone (micrite: M; peloids: P). 9 m above the section base. Scale bar is 2 mm. **E)** Photomicrograph illustrating two different layers of infiltrated fine sediments within Facies 2 boundstone (red dotted line). Ostracods (o), stromatoporoids (s), and crinoids (c) are present. 9 m above the section base. Scale in bar is 2 mm. **F)** Photomicrograph of the encrinitic Facies 3. Note the presence of infiltrated micrite locally present as geopetal sediment and replaced by blue stained dolomite crystals. 10 m above the section base. Scale bar is 5 mm. **G)** Photomicrograph showing Facies 3 grainstone with crinoidal material and their syntaxial overgrowth. Note the dolomite replacement as seen in F. 9.7 m above the section base. Scale bar is 500 µm. **H)** Photomicrograph showing crinoidal grainstone with abundant algae and calcimicrobe (Microfacies 3a) including *Girvanella* (G), *Rhabdoporella pachyderma* (Rp), *Rhabdoporella stolleyi* (Rs). 9.5 m above the section base. Scale bar is 500 µm.

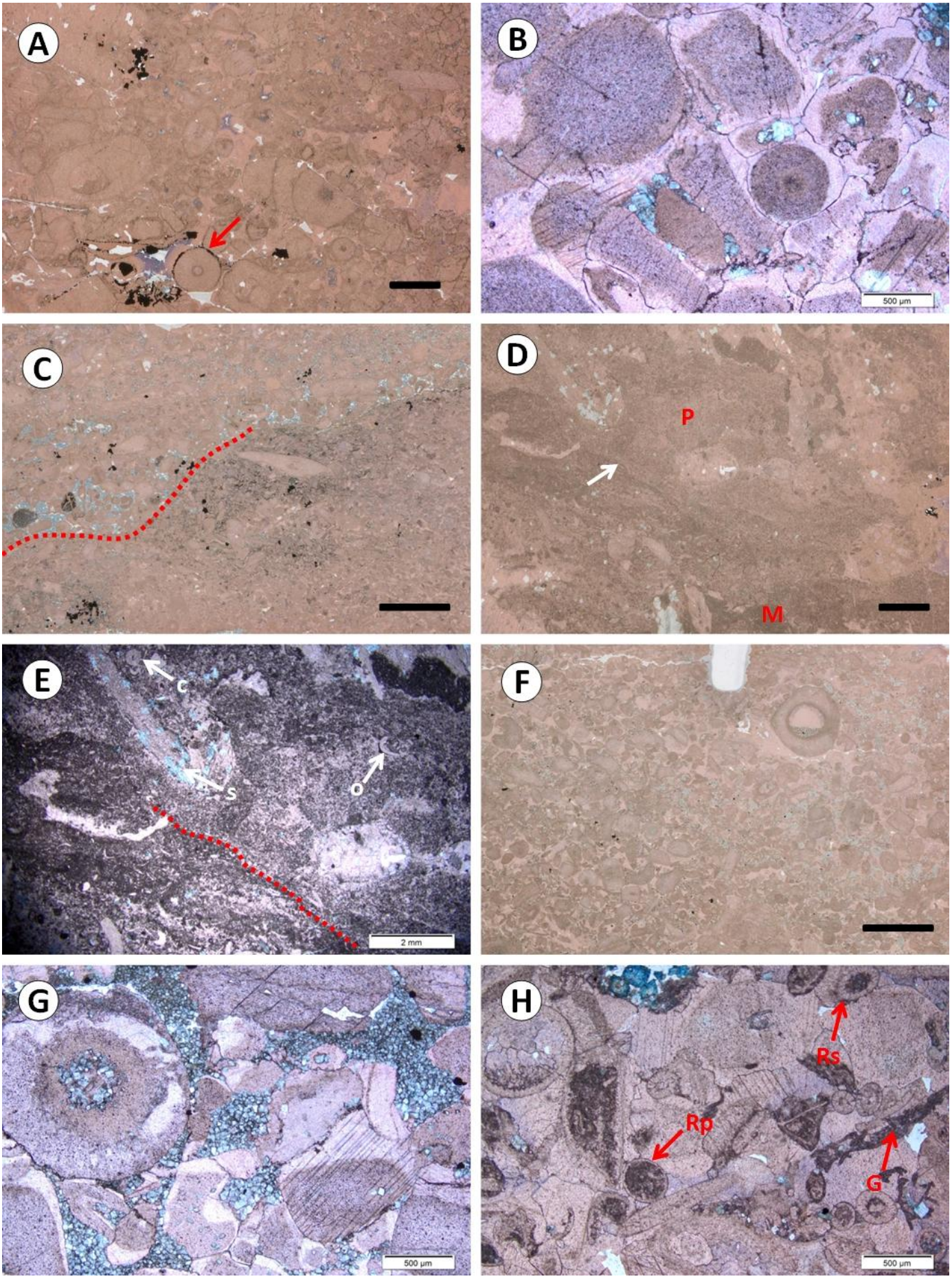
A
B
500 µm
C
D
P
M
E
c
s
o
2 mm
F
G
500 µm
H
Rs
Rp
G
500 µm

3.3 - Facies 3 – Encrinites interbedded with Calcareous Shale

This facies is similar to Facies 1, but is finer grained (Plate 2A), more thinly bedded (5 to 15 cm) and bioturbated, less amalgamated, and has a greater textural range (packstone/grainstone/rudstone). Distinctive greenish fissile calcareous shale partings (0.1 to 1 cm) are common, on average, every 10-15 cm (Plate 2B). In this facies, encrinites are light grey to light brown, but are commonly darker than Facies 1 encrinites (Plate 2B). Other fossils include brachiopods, bryozoans, stromatoporoids and corals. In thin section, encrinites show up to 30% of blue-stained, ferroan dolomite crystals replacing selectively the micritic matrix (Plates 3F, 3G and 3H). Furthermore, this matrix shows local geopetal structures (Plate 3F) indicating an infiltration of micrite and peloids after crinoidal sand deposition. Calcite cement is dominated by non-ferroan syntaxial overgrowth filling the space left by the matrix (Plate 3G).

Facies 3 represents sediments deposited on a more distal mid-ramp environment than Facies 1 as evidenced by its lesser amalgamated character, greater bioturbation, and preservation of shale partings between individual storm events. Furthermore, finer grained material, lime mud and peloids, is common and shows infiltration after deposition supporting a more distal mid-ramp environment.

3.3a - Microfacies 3a – Algal-Rich Encrinites

This microfacies is only recognizable in thin section and characterized by abundant calcareous algae and calcimicrobe. This microfacies occurs in the basal two meters of the Chicotte Formation below and above Facies 2 bioherms and biostromes. The distinctive stratigraphic position of this microfacies is observed also in other basal Chicotte sections (A. Desrochers pers. comm. 2012); thus providing a regional marker level for the basal Chicotte Formation. The encrinitic microfacies is a crinoidal packstone/grainstone, with a variable amount of dolomite crystals that have partially replaced the matrix and a remarkable content (up to 20 %) in calcareous algae and calcimicrobe (Plate 3H) including: *Girvanella*, *Rhabdoporella pachyderma*, *Rhabdoporella stolleyi*, *Rothpletzella* (described as *Sphaerocodium* in Héroux et al., 1997 and Mamet et al., 1992).

The presence of calcareous algae and calcimicrobes indicated a depositional environment within the photic zone. Microfacies 3a represents a distinctive depositional phase of Facies 3 when conditions were more favorable for the growth of algae and calcimicrobe. One possible scenario was

a brief, but effective shut down of siliciclastics (see discussion below) and expansion (i.e. deepening) of the photic zone on the ramp.

3.4 - Facies 4 – Bioclastic Packstone/Grainstone Facies with Calcareous Shale Interbeds

This facies consists of thin to thick bedded (5 to 40 cm), lenticular to subtabular, discontinuous, sharp-based bioclastic packstone/grainstone/rudstone with thin calcareous shale interbeds (Figs. 3, 4, 5, and 6 and Plates 1A, 1D, 1E, 1G, and 4A). These limestones are light brown to green grey. Beds are commonly graded (fining upward), but locally bioturbated with distinctive *Thalassinoides* burrows near their tops. Symmetrical LWR are present at regular intervals (Figs. 5 and 6, Plates 4A and 4B), with interval cross-stratification (Plate 4C) and represent continuous marker beds at the outcrop scale. These LWR are up to 15 cm high with wavelength of 50 to 70 cm. Their crests are oriented roughly N/S implying an E/W wave current direction. Additional paleocurrent data, provided by long crinoid stems, are oriented preferentially N/S and therefore perpendicular to the inferred E/W paleocurrent direction (Plate 4D). Major skeletal grains are crinoids (Plate 5A), brachiopods, rugose and tabulate corals, bryozoans and ostracods. Trilobites, stromatoporoids and gastropods are also present. Intraclasts are locally abundant and made of wackestone or packstone fragments. Note that this lithology is only preserved as intraclasts in our sections. Intraclastic and bioclastic rudstones are present in this facies (Plates 4A and 5B). The intraclast size varies from gravel up to boulder. Furthermore, intraclasts have darker edges defined by a pyrite rich zone (Plate 5B). Extensive shale rip-up clasts are also present. Matrix, if present, is partially replaced by coarse dolomite crystals. Peloids are locally abundant in the matrix. Calcareous shale interbeds may represent locally up to 50 % in volume (uppermost Section 1, Fig. 3). Calcite cement is mainly drusy, but syntaxial overgrowth is also common around crinoidal debris. Both calcite cements are largely non-ferroan with a ferroan phase locally present as the final pore-occluding phase.

Facies 4 is present in all sections ranging from those closer to the basin margin (sections 1 to 3) to the more distal Section 4 (see Figs. 3, 4, 5 and 6). Within the Facies 4, we can differentiate two microfacies 4a and 4b. Microfacies 4a is present in the upper part of the basin margin sections (see Figs. 3 and 5). Microfacies 4b is found only in Section 3 (see Fig. 5).

3.4a - Microfacies 4a – Sandy Bioclastic Packstone/Grainstone

This microfacies is characterized by its high siliciclastic content. Siliciclastic particles consist of very fine, angular quartz grains (Plates 5D and 5E), which are mixed with carbonate grains and matrix. Siliciclastics are locally important forming distinct laminae within the grainstones (Plate 5E). This microfacies shows a gradual contact with HCS sandstones (Facies 6).

3.4b - Microfacies 4b – Algal-Rich Bioclastic Packstone/Grainstone

This microfacies in thin section is characterized by the presence of abundant calcareous algae (up to 20 % in total) and calcimicrobe. This microflora (Plate 5C) comprises several taxa including: *Girvanella*, *Rhabdoporella*, *Anticostiporella*. Microfacies 4b differs from the algal-rich encrinites (Microfacies 1a) by a different microfloral content and a cleaner grainstone texture. This microfacies is possibly present in the uppermost part of Section 1.

Facies 4 represents storm-influenced sediments that were deposited along a distal mid-ramp with some cleaner grainstones deposited during stronger storm events. This depositional setting is evidenced by the presence of symmetrical LWR, sharp scoured bed bases, normal grading within individual beds, and discontinuous to lenticular bedding (see sections 4.5 and 4.6). These sedimentary structures are indicative of the combined action of storm wave agitation and return bottom current. Wave agitation kept sediment in suspension whereas return unidirectional current was, then, able to transport them downramp. Several lenticular beds occurring at the same stratigraphic level represent a single event when the front of the return flow became unstable and separated into smaller flow fingers. The presence of wackestone/packstone intraclasts and rip-up clasts indicate some erosion during the progression of the combined flow down ramp. Wackestone/packstone facies, being poorly represented in our section, represent minor intensity storm deposits which are reworked systematically by stronger storms. Thus, limestone beds represent the activity of storms and their relative abundance can be used as a proximal-distal proxy. The deposition of calcareous shale implies fair weather conditions between storm events allowing the settling of the fine grained material in suspension. Similar interpretations have been proposed by Long (2007) with the bioclastic sandstones and intraclast conglomerates, as well as Triassic storm deposits in southern Spain (Pérez-López and Pérez-Valera, 2011; their Facies A).

Plate 4: Field photographs of Facies Association 2. White dashed lines separate different facies. Red arrows point out specific features. **A)** Field photograph showing bioclastic packstone/grainstone with calcareous shale interbeds (Facies 4) along a small coastal cliff. Note the bed with LWR used as a local marker point (red arrow) above a massive bed of intraclast-rich and bioclastic rudstone. 4.7 to 6.5 m above the base of Section 4. Scale in a meter. **B)** Field photograph illustrating symmetrical LWR (50 to 70 cm wide and up to 15 cm high) on a bedding plane. 4.5 m above the base of Section 4. Scale is a 10 cm ruler. **C)** Field photograph showing well developed HCS in cross section (see the sketch provided below) within a LWR local marker bed. 5.7 m from the base of Section 4. Scale bar is 10 cm ruler. **D)** Field photograph illustrating crinoid stems (up to 5 cm long) with a preferred N/S orientation on a bedding plane. ~4 m above the base of Section 4. Scale is 10 cm. **E)** Field photograph showing in cross section view subnodular bioclastic packstone/grainstone with thin calcareous shale interbeds (Facies 5). ~1 m above the base of Section 1. Scale is a hammer. **F)** Field photograph showing HCS sandstone (Facies 6) overlain by sandy packstone/grainstone (Facies 4a). Note the very thin laminations in the sandstone. 6 m above the base of Section 1. Scale is a hammer. **G)** Field photograph showing *Chondrites* burrows on a bedding plane in Facies 6. 8.5 m above the base of Section 1. Scale bar is 5 cm. **H)** Field photograph exposing thin HCS beds separated by shale interbeds in cross section (Facies 6). 1.2 m above the base of Section 3.

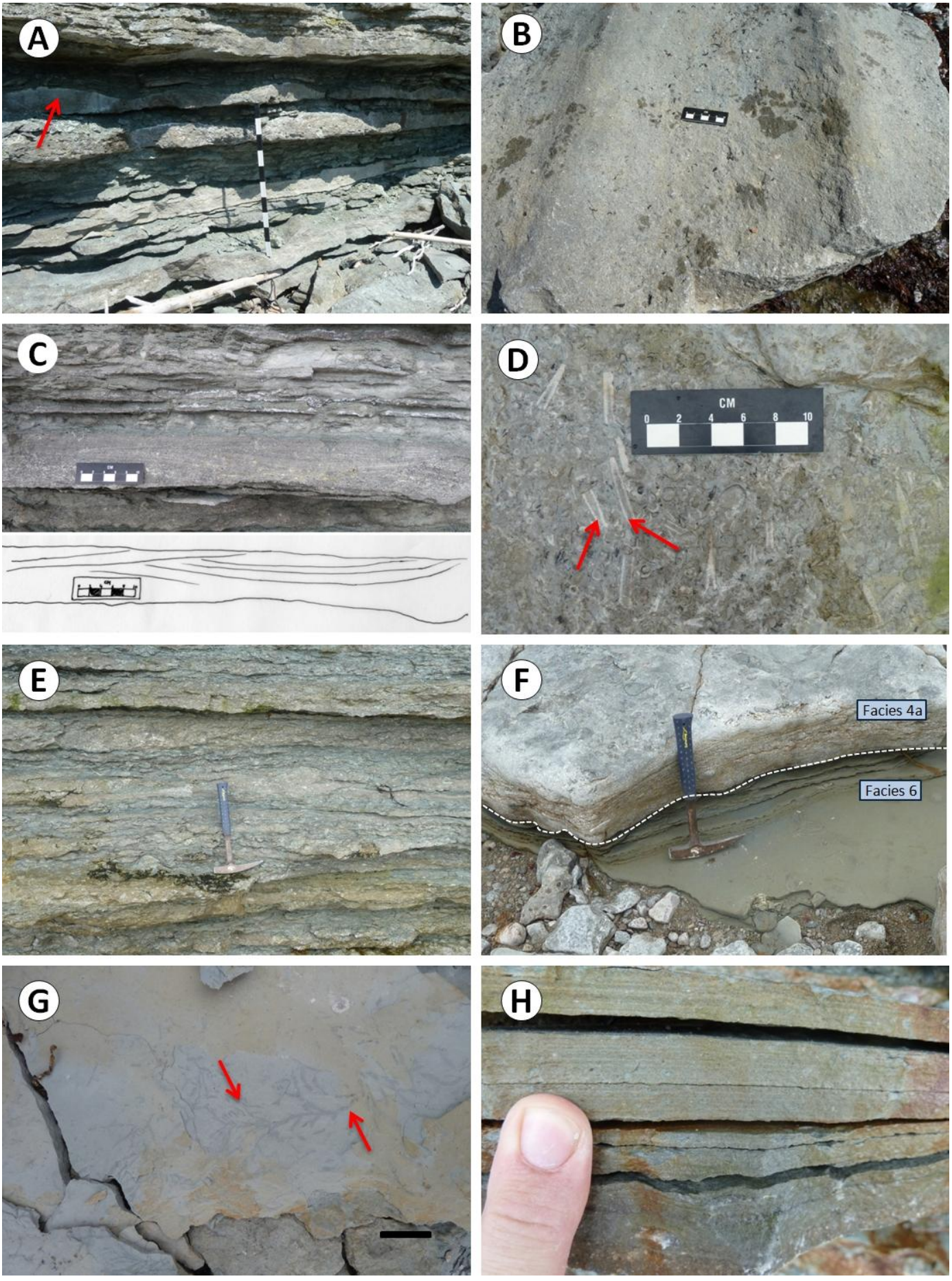
A
B
C
D
CM
0 2 4 6 8 10
E
F
Facies 4a
Facies 6
G
H

Plate 5: Photomicrographs of Facies Association 2. Red arrows point out specific features. **A)** Photomicrograph illustrating bioclastic grainstone of Facies 4. Note the rounded crinoidal fragments and some larger solitary rugose coral. 3.2 m above the base of Section 4. Scale bar is 5 mm. **B)** Photomicrograph of bioclastic rudstone showing large polymictic intraclasts (1 to 3). 5.5 m above the base of Section 4. Scale bar is 2 mm. **C)** Photomicrograph showing various calcareous algae (Facies 4b) including: *Anticostiporella* (A) and *Girvanella* (G). Section 3 at its base. Scale bar is 500 µm. **D)** Photomicrograph illustrating packstone/grainstone with abundant crinoids and ostracods (Facies 4a). Note the presence of fine sand quartz particles. 10 m above the base of Section 1. Scale bar is 500 µm. **E)** Photomicrograph showing alternating laminations of fine grained siliciclastic and bioclastic material (Facies 4a). Pyrite is present as black, opaque, square shaped. 1.2 m above the base of Section 3. Scale bar is 2 mm. **F)** Photomicrograph of Facies 6 sandstone showing fine grained quartz particles in white, dolomite in blue, and micas in brown/green (red arrow). 5.8 m above the base of Section 1. Scale bar is 200 µm.

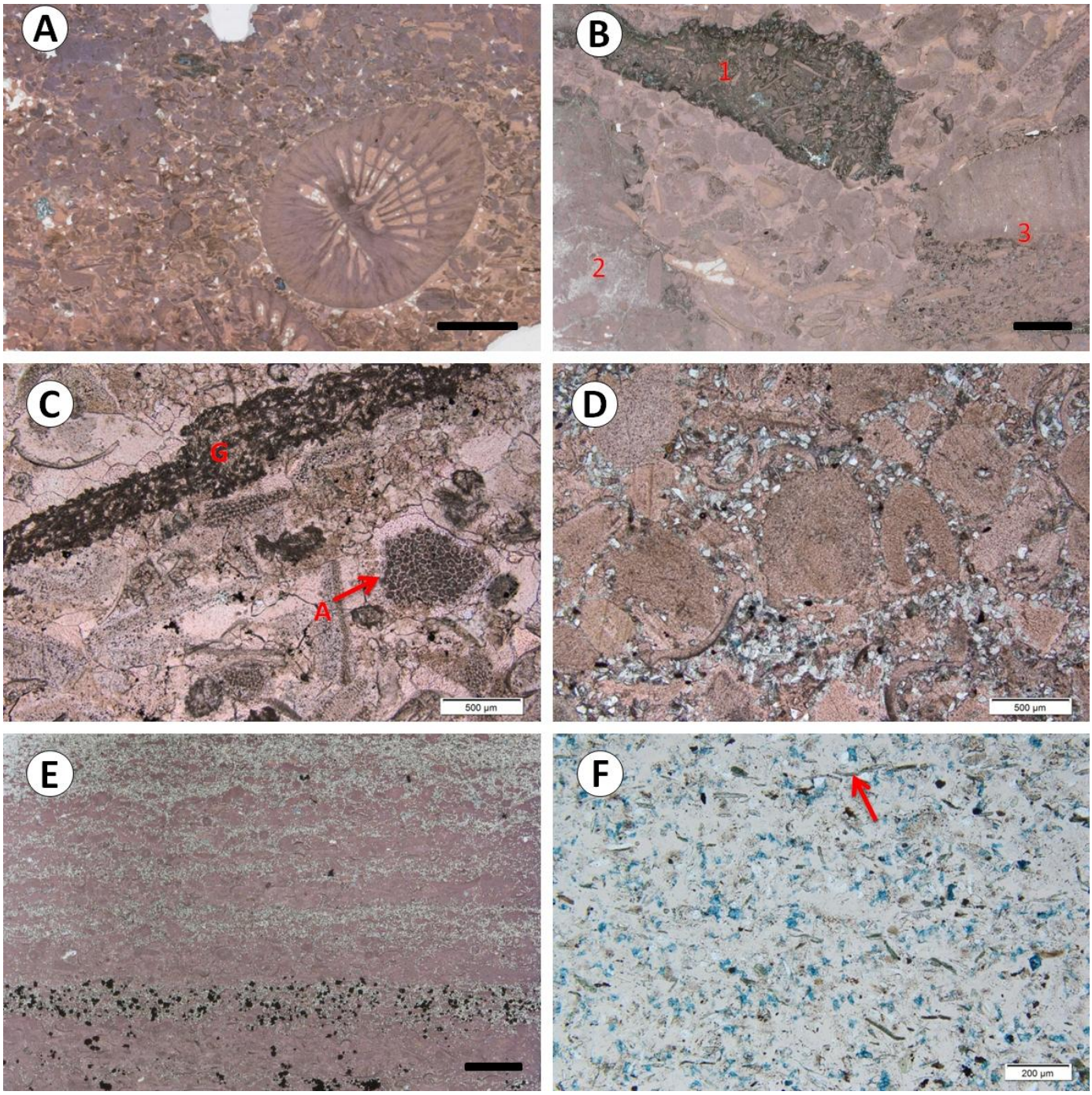
A
B
1
2
3
C
G
A
500 µm
D
500 µm
E
F
200 µm

Microfacies 4a represents sediments accumulating under the same conditions than those of Facies 4. Nevertheless, a significant influx in siliciclastic sand was possible during episodic river discharge. Note that the siliciclastic influence is more important on the east side on the island implying the source in this region (see Section 5.2). Microfacies 4b with its microfloral abundance indicates that calcareous algae accumulated at shallow water depths under saturated light conditions. A similar scenario as the above microfacies 3a could be envisaged.

3.5 - Facies 5 – Nodular Bioclastic Packstone/Grainstone interbedded with Calcareous Shale

This facies consists of thin to medium bedded (5 to 15 cm), nodular to tabular, discontinuous, bioturbated bioclastic packstone/grainstone with thin (1 to 5 cm) calcareous shale interbeds (Figs. 3 and 5, Plates 1A and 4E). The more tabular beds are typically sharp based. Limestone beds are brownish grey whereas shale interbeds are greenish grey. The shale interbeds represent up to 40% of the stratal volume. Skeletal grains in limestone beds are dominated by brachiopods, but other taxa are also present including: crinoids, bryozoans, ostracods, and trilobites. A lime mud matrix is locally present and partially replaced by dolomite crystals. Cement is characterized by non-ferroan drusy calcite and syntaxial overgrowth. Facies 5 is present at the basin margin section (Section 1; see Fig. 3), but rare or absent at more distal sections (Section 4; see Fig. 6).

Limestone beds in Facies 5 display similar features to those in Facies 4, but its thinner, nodular bedding and more abundant lime mud matrix are indicative of a more distal storm-influenced mid-ramp, or even an outer ramp setting. Ubiquitous bioturbation and poorly developed sedimentary structures suggest also a more distal ramp setting. Furthermore, sharp-based beds and coarse-grained rudstone are rare when compared to Facies 4. The deposition of calcareous shale as interbeds implies fair weather conditions between storm events allowing the settling of the fine-grained material in suspension.

3.6 - Facies 6 – HCS Sandstone interbedded with Calcareous Shale

This facies consists of fine grained HCS sandstone with thin (2 to 5 cm) calcareous shale interbeds (Figs. 3 and 5 and Plates 1B, 1E, 4F, 4G, and 4H). Individual sandstone bed, up to 15 cm

thick, shows a sharp-scoured base overlain typically by a coarse bioclastic lag. HCS displays usually one coset with wavelengths ranging from 3 to 5 m. Bioturbation, mainly *Chondrites*, is locally present (e.g. Section 1). In thin section, sandstones consist of abundant very fine sand size, angular quartz grains, but micas, mainly muscovite and biotite, are common (Plate 5F). Micrite and peloids are also present. Facies 6 is only present at basin margin sections (e.g. sections 1 and 3; see Figs. 3 and 5).

HCS forms above storm wave base (SWB) under combined flows with a strong oscillatory component but a weak unidirectional component (Dumas and Arnott, 2006; see also section 4.4). They form typically on the transition zone or distal mid ramp. In addition, their preservation suggests deposition below fair weather wave base (FWWB) in order to avoid wave reworking. The presence of calcareous shale interbeds suggests also that Facies 6 formed under the FWWB. Furthermore, the abundance of micas suggests a proximal sediment source and especially, as noted in Facies 4a, on the east side of the island where more siliciclastic sediments outcrop. Thus, Facies 6 is interpreted as sediment deposited on the distal mid-ramp. Similar deposits have been identified within the Anticosti succession with a similar interpretation, as well as, oolithic grainstones from southern Spain (Pérez-López and Pérez-Valera, 2011; their Facies D).

3.7 - Facies 7 – Calcareous Shale

This facies consists of thin to thick bedded (5-30 cm), fissile to subnodular calcareous shale (Figs. 3 and 6, Plate 1B). Some samples (once grinded) show a significant reaction with hydrochloric acid. We distinguish clearly two groups, a carbonate-rich (FC1, 4 and 6) and a carbonate-poor (FC-2, 3 and 5). The variations in the carbonate content show no correlation with stratigraphy or geography, it is thus interpreted as diagenetic in origin.

Facies 7 represents sediment deposited during fair weather conditions on the outer ramp where the seafloor was rarely affected by storms as evidenced by the high amount of calcareous shale and the absence of coarser sediment. Constant siliciclastic sediment influx was probably coming from one or several rivers situated eastward of the outcrop belt (see Section 5.2) and when the conditions were quiet enough, the suspended load was able to settle on the mid to outer ramp, with a greater preservation potential downramp. Similar interpretations were mentioned for Anticosti

Silurian marls and Triassic fair-weather deposits from southern Spain (Long, 2007; Pérez-López and Pérez-Valera, 2011).

3.8 - Facies 8 – Bioturbated Mudstone/Wackestone with Bioclastic Packstone/Grainstone Interbeds

This facies consists of thin- to thick-bedded (5 to 40 cm) lenticular, highly discontinuous, sharp-based, bioclastic packstone/grainstone/rudstone, interbedded with subnodular bioturbated mudstone/wackestone (Figs. 4 and 6, Plates 1D, 1E, 1G, 6A, and 6B). The coarser grained limestone beds are lenticular, locally channelized and laterally discontinuous (Plates 6A and 6B). The grains in these limestones range in size from bioclastic-rich gravel to peloid-rich silt (Plate 7D). Within a single bed, the coarser bioclastic layer is graded at the base while the capping peloid-rich layer is parallel laminated (Plate 6B). Symmetrical LWR present at regular intervals in the lower Pavillon Member (Figs. 4 and 6) can be used as local marker beds. The associated fauna is diversified at the outcrop scale, but can be more monospecific (e.g. brachiopods and bryozoans) at the bed scale (Plates 4D and 7C). Major skeletal grains are brachiopods, crinoids, rugose and tabulate corals, bryozoans, trilobites, and ostracods (Plates 6D, 6F, 7B, and 7C). Mollusks and stromatoporoids are also present. Elongated crinoid stems are present at the base of some beds forming an obliteration deposit (Plate 6E). A lime mud or matrix is locally common and partially replaced by dolomite crystals. Calcite cement is drusy, but syntaxial overgrowth is present around crinoidal material. Calcite cement is largely non-ferroan with rare ferroan calcite cement present as the final pore-occluding phase. Associated mustones/wackstones may represent up to 70 % in volume.

Sharp-based, lenticular fining-upward coarser grained limestones represent distal mid-ramp sediments deposited under a wave-enhanced sediment-gravity flow relative to episodic storm events (see section 4.6). Gravity flows are, then, produced by the combined action of storm wave agitation and return bottom current. Wave-induced oscillatory flows keep sediment in suspension in the boundary layer (~10 cm thick) just above the sea floor (Plint, 2010). The return unidirectional current, together with gravity, is subsequently able to transport the sediment downramp (see section 4.6). Different lenticular beds at the same stratigraphic level represent the same event as the gravity flow front became unstable and separated into several smaller fingers. Furthermore, building of symmetrical LWR is believed to be storm-influenced (for detail, see section 4.5). Highly bioturbated mudstone/wackestone represents the background sedimentation between individual storm events.

Plate 6: Field photographs of Facies Association 3. White dashed line separates different facies. Red and white arrows point out specific features. **A)** Field photograph of bioturbated mudstone/wackestone (Facies 8) with increasing lenses (red arrow) of bioclastic packstone/grainstone toward the top (Facies 9). Basal three meters of Section 4. Scale is a meter. **B)** Close-up of A showing in cross section a lenticular calcarenite bed (Facies 8): distal wide gutter cast. Note the graded nature of this bed. 2 m above the base of Section 4. Scale is a meter. **C)** Field photograph illustrating on a bedding plane the darker walls of burrows in Facies 9. 1 m above the base of Section 2. **D)** Field photograph showing various fossil fragment on a bedding plane including brachiopods (mainly orthids) trilobite (red arrows) and branching bryozoans (white arrow). 2.5 m above the base of Section 2. **E)** Field photograph illustrating an obliteration with a concentration of crinoid stems parallel to bedding overlain by sharp-based bioclastic grainstone (Facies 8). 2.5 m above the base of Section 4. **F)** Field photograph showing a large favositid tabulate coral colony in Facies 8. 3 m above the base of Section 4. Scale is 50 cm.

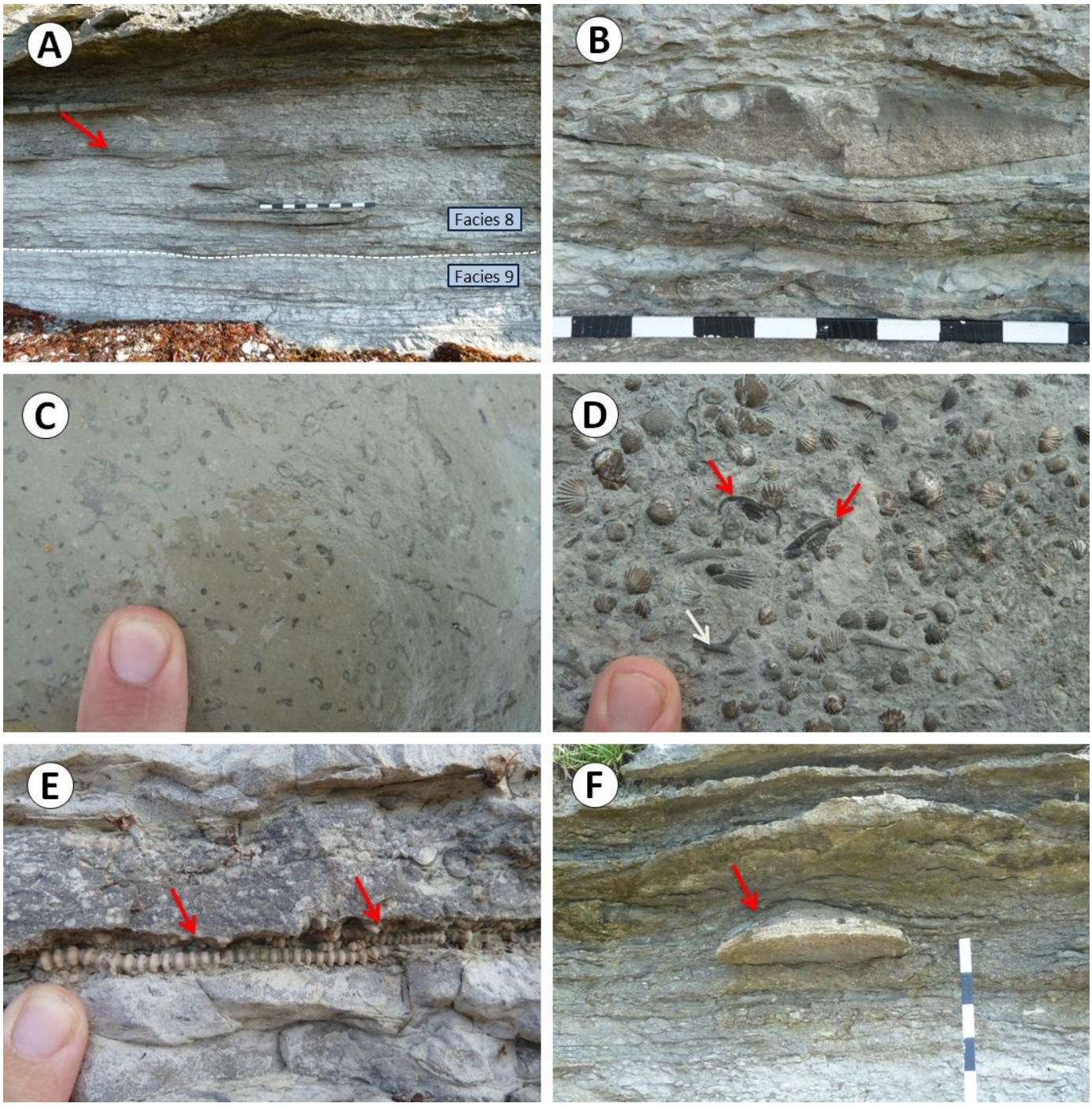
A
Facies 8
Facies 9
B
C
D
E
F

Plate 7: Photomicrographs of Facies Association 3. Red and white arrows point out specific features. **A)** Photomicrograph showing bioturbated dolo-mudstone/wackestone (Facies 9). 1 m above the base of Section 2. Scale bar is 2 mm. **B)** Photomicrograph illustrating abundant brachiopods in Facies 8 packstone. 1.5 m above the base of Section 2. Scale bar is 5 mm. **C)** Photomicrograph showing bioclastic grainstone in Facies 8 with brachiopods together with some bryozoans (white arrow) and gastropod (red arrow). 4.8 m above the base of Section 2. Scale bar is 2 mm. **D)** Photomicrograph showing fine grained peloid rich grainstone in Facies 8. 1.6 m above the base of Section 4. Scale bar is 500 µm.

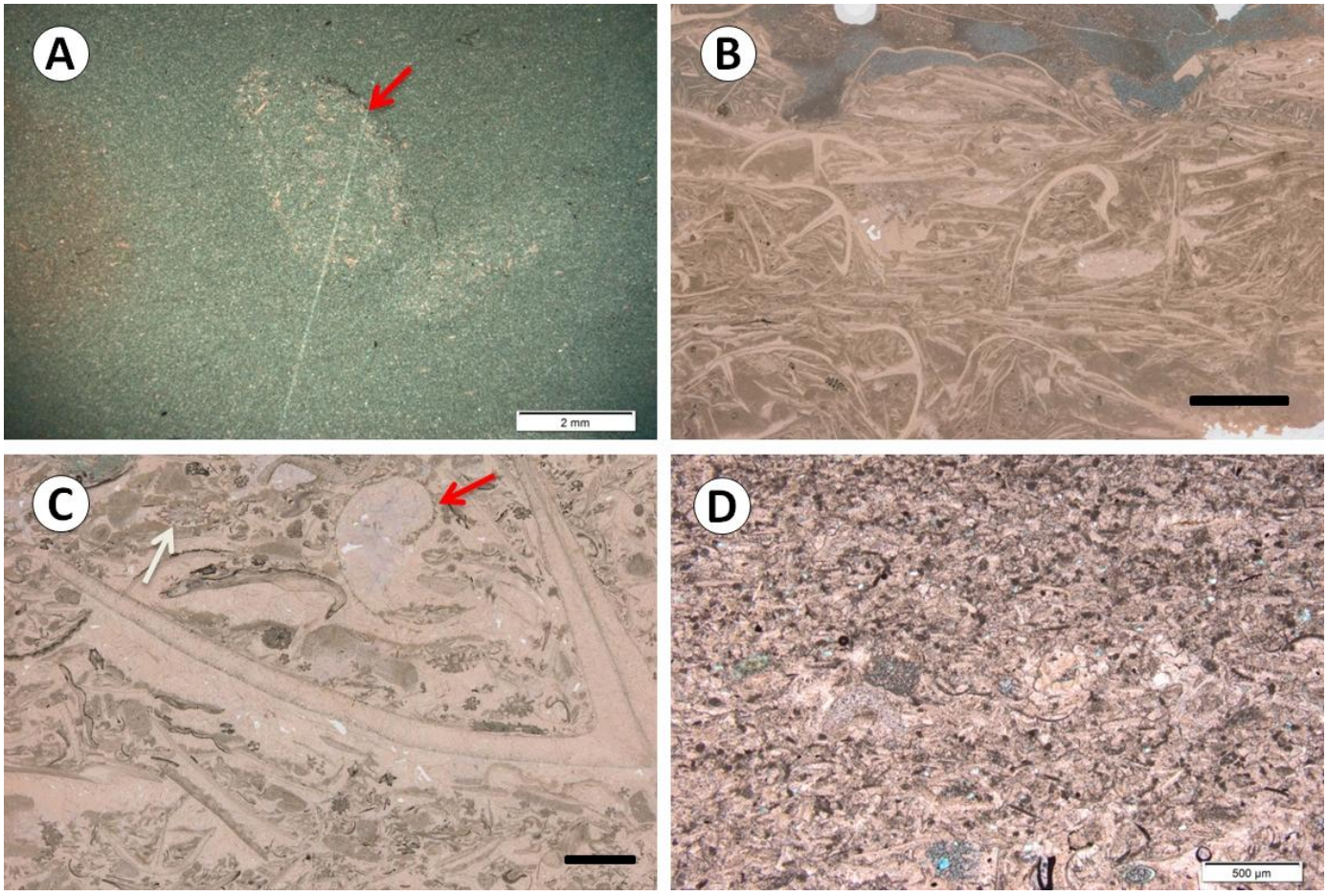
A
2 mm
B
C
D
500 µm

A hydrodynamic segregation of the fauna is evidenced by the monospecific beds (see Section 4.3) where brachiopods and bryozoans, having specific hydrodynamic characteristics, are separated from the rest of the fossils. Anticosti sharp based graded micrites have been interpreted as storm-generated beds (Long, 2007). Furthermore, beds from ancient mud-rich outer-shelf to basinal successions (Cleveland Ironstone, Jurassic, UK, and Mowry Shale, Cretaceous, USA) have been reinterpreted as storm-generated high-energy events (Macquaker et al., 2010).

3.9 - Facies 9 – Bioturbated Mudstone/Wackestone

This facies is thin bedded (5 to 10 cm thick), tabular to subnodular, bioturbated mudstone/wackestone (Figs. 4 and 6, Plate 6A). Burrows are outlined by darker borders (Plate 6C). In thin section, the burrow edges are pyrite-rich (Plate 7A). Skeletal grains are rare, but bioclasts-rich, lenticular laminae are present. Skeletal grains are brachiopods together with crinoids, ostracods, bryozoans, and trilobites. The lime mud matrix, or micrite, is partially replaced by dolomite crystals (Plate 7A).

Facies 9 represents lime mud transported in suspension downramp during storm events and deposited in a relatively quiet setting near the base of, or even deeper than, the SWB. This suggests deposition in a distal mid-ramp to outer ramp setting. Similar facies on Anticosti and in southern Spain have also been interpreted as post-storm deposits (Long, 2007; Pérez-López and Pérez-Valera, 2011).

4 - Associated Sedimentological Features

Facies listed in Table 1 comprise distinctive sedimentary structures including: gutter casts, sharp basal contacts, shell beds, hummocky cross-stratification (HCS), large wave ripples or LWR, wave-enhanced sediment-gravity flow deposits and erosional surfaces.

4.1 - Gutter Casts

Gutter casts are common in the Pavillon Member of the Jupiter Formation at the base of some coarse grained, graded grainstone/rudstone bed. These gutter casts are U-shaped in cross section and well oriented with some bifurcations in plane view. They are shallow and relatively wide in the lower part of the Pavillon Member (Plate 6B), but deeper (up to 10 cm) in the upper part of the Pavillon Member. Their infill displays a basal conglomeratic lag and an overall normal grading.

Gutter casts are cut and fill structures created by offshore-oriented storm flows preserved typically in proximal storm facies (Myrow, 1992). In the more nearshore HCS facies, these structures are roughly oriented perpendicular to the shoreline whereas more offshore, they tend to be shore-oblique and smaller (Plint, 2010). Furthermore, bioturbation and colonization of the gutter surface by encrusting organisms indicate that erosion and filling may be two separate events (Sami and Desrochers, 1992). In our case, erosion and subsequent filling resulted from the same event. Wide and shallow gutter casts are interpreted to represent relatively distal storm flows (see also section on wave enhanced gravity flows) whereas sinuous, deeper gutter casts represent more proximal flows.

4.2 - Sharp Basal Contacts

Sharp contacts are present at the base of individual coarse-grained limestone beds in both Pavillon and Brisante members. Contacts are sharp with little or no erosional relief, but are locally more irregular and highly sculptured (Plate 3C).

The development of these structures is due to erosion prior to deposition. During the peak storm, the dense and high-energy combined flow progressing downramp erodes into the underlying soft substrate. Irregularity of the surfaces is probably the result of selective erosion of less cohesive parts of the substrate (Sami and Desrochers, 1992).

4.3 - Shell Beds

Shell beds, 5-15 cm thick, are laterally discontinuous and usually common in bioclastic calcarenites throughout the lower Pavillon Member. Several shell beds (examples from Section 2 in

Plate 6D), which were first recognized by Copper and Long (1990), can be traced for several tens of meters laterally. Associated fauna are rarely found *in situ*.

Shell beds are an accumulation of shells, called dynamic shell lags by Dott (1983), due to transport and concentration where energetic flows, have winnowed the finer-grained material. By contrast, *in situ* brachiopods are locally present at the top of some bioclastic calcarenites. These calcarenites played a key role in making suitable substrates for sessile fauna habitation.

4.4 – Hummocky Cross-Stratification (HCS)

HCS sandstones, 5-10 cm thick, are present in the upper Pavillon Member. Beds are sub-tabular, discontinuous with a sharp erosional base. HCS are nearly isotropic and have wavelengths of 3-4 m and amplitudes of 5-15 cm. Parallel laminae dip at a very low angle, but internal truncation surfaces or amalgamation are rare. HCS occurs in fine grained sand.

HCS forms above the SWB where aggradation rates during storms are high enough to preserve hummocks (Dumas and Arnott, 2006). Isotropic HCS forms under combined flow regime with a weak unidirectional flow whereas anisotropic HCS forms with a stronger unidirectional current (Dumas and Arnott, 2006). Thus, anisotropic HCS is interpreted to form in more proximal environment than isotropic HCS. However, Yang et al. (2006) showed that HCS wavelength is indirectly related to water depth: wavelengths are shorter on both sides of the wave breaking point. In our case, HCS is, as in Dumas and Arnott (2006), interpreted to have formed in a relatively distal ramp setting by combined flow with a weak unidirectional flow. Nonetheless, our HCS wavelength appears to be larger than equivalents in the literature (Plint, 2010; Yang et al., 2006; Dumas et al., 2005). Such wavelength (3-4 m) implies either a shallow environment according to Yang et al. (2006) or extremely large waves; the latter being more consistent with our more distal mid-ramp depositional interpretation.

4.5 - Large Wave Ripples (LWR)

Symmetrical to slightly asymmetrical LWR are common throughout the Pavillon Member. Their spacing varies between 50 cm and 80 cm and height can reach up to 15 cm (Plates 4A and 4B).

They are commonly coarse grained (coarse sand and gravel) with the coarser fraction more abundant in the troughs.

Ripples are mainly dependent on grain size and flow properties, grain size playing more important role (Cummings et al., 2009). Until now, no HCS has been reproduced in laboratory in coarse sand or gravel (Dumas pers. comm. 2012). Instead, strong oscillatory flows can produce large symmetrical oscillatory ripples (Dumas et al., 2005). Thus, our LWR structures are large oscillatory ripples and occupy the same hydrodynamic field as the hummocky zone in finer sediments. Furthermore, LWR beds display low-angle cross-stratification typically seen in the hummocky field zone (Dumas and Arnott, 2006). The slight asymmetrical character is then related to the presence of a combined flow, where the relatively weak unidirectional current allows the bedform to migrate preferentially. Alternative interpretation involves internal waves at the slope break where oceanic currents interact with the superficial currents and create an internal instability interface. Nevertheless, no evidence for a break in the slope was noticed so far, the paleoslope is believed to be further southward.

4.6 - Wave-Enhanced Sediment-Gravity Flow Deposits

Upward fining beds, 5-30 cm thick, are common throughout the Pavillon Member. These beds are sharp based and locally lenticular and discontinuous. Their internal vertical sequence consists of, from base to top: (i) a sharp erosional base showing sole marks as wide gutter casts filled with a shell/intraclast lag; (ii) fining-upward coarse sand and gravel size bioclasts (mainly reworked shells); (iii) sub-horizontal planar laminated peloid calcisiltite in which HCS is poorly developed.

A carbonate ramp is typically not steep enough to produce gravity flow deposits; especially when a coarse sand to gravel fraction is present. A possible way, however, to produce these deposits is by the interaction with a combined flow during a storm event. The development of a sediment gravity flow begins with wave-induced turbulent resuspension (Macquaker et al., 2010) where increasing wave-generated turbulence destabilizes density stratification (Friedrichs and Wright, 2004) (Fig. 7). Then a downramp-flowing sediment suspension progresses according to a pressure gradient (i.e. wave-enhanced sediment-gravity flow, WESGF). Furthermore, the gravity flow head becomes unstable during the advanced stage of a sediment-gravity flow and divides itself into several arms according to Rayleigh-Taylor instability rule (Chen et al., 1994). This character is

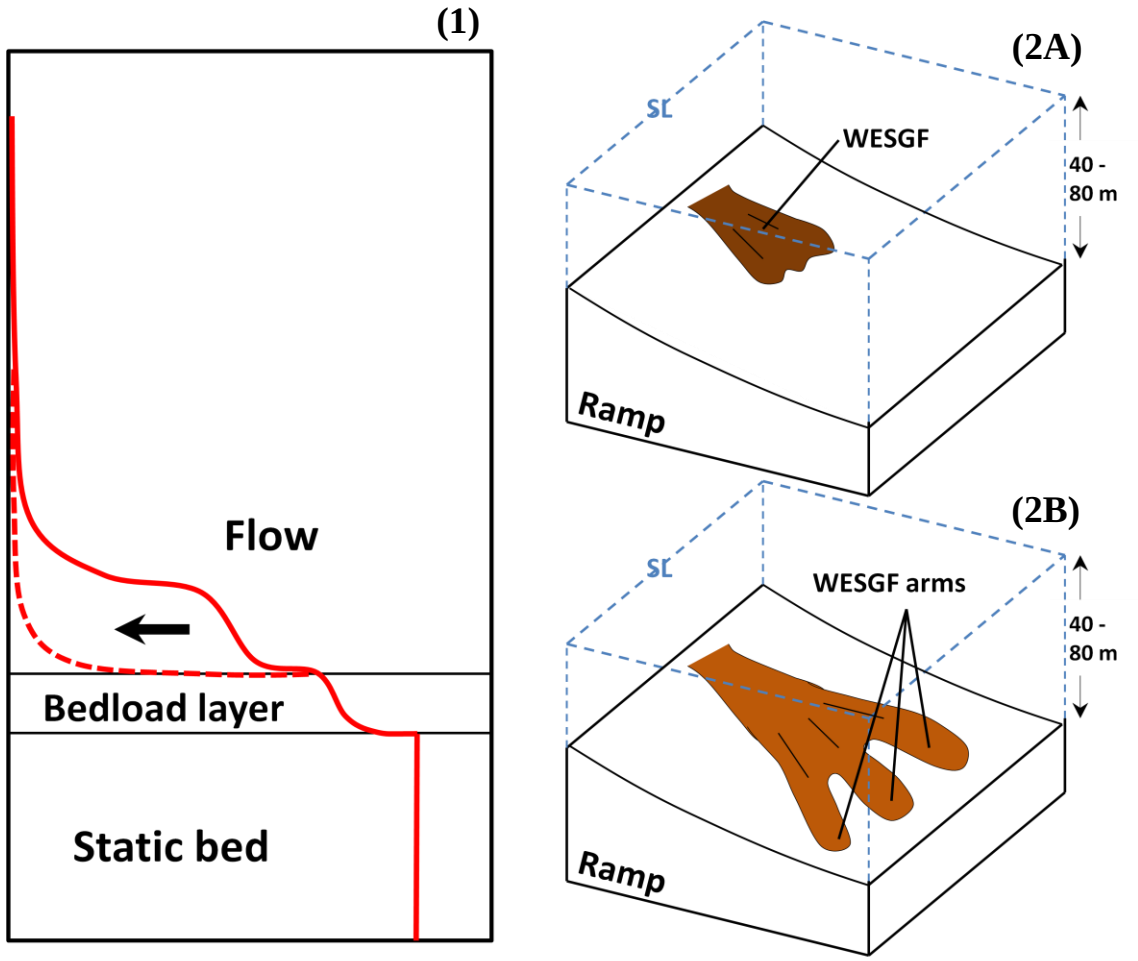

Figure 7: (1) Hypothetical sediment concentration profile from the sea floor to the base of a clear-water flow (dashed line) and a turbidity current (solid line) (Arnott, in press); and (2) schematic evolution of a WESGF. (1) Initially, high sediment concentration at the base of the flow prevents the development of a steep density gradient between the bedload layer and the base of the flow. As the flow progresses, concentration decreases (arrow) and the density gradient becomes sufficiently steeper to generate instabilities and eventually ripples grow. In this case, flow speed decreased sufficiently and reached the lower plane bed hydrodynamic field before developing the density interface. (2A) Dense initial WESGF progresses downramp developing a wavy front eventually separating into several, less dense arms (2B) according to Rayleigh-Taylor instability. (SL is for sea-level and 40 – 80 m is the estimated water depth)

well illustrated by the presence of shore-perpendicular, highly discontinuous and lenticular beds (gutter cast in Plate 6B) associated with our deposits. The graded nature of these deposits implies a gravity-driven deposition (Arnott, pers. comm. 2012) which can be compared to a turbidite. With only gravel, coarse sand and silt size particles, the coarser grained fraction was quickly deposited in a massive and graded unit ((i) and (ii); Bouma turbidite unit a), but evolved directly into the deposition of plane bed peloidal silts (iii) equivalent to Bouma turbidite units b and d, without the usual development of ripple or dune cross-stratification (Bouma turbidite unit c). Arnott (in press) argued that, contrary to plane beds, and in the case of a turbidite, a sufficiently sharply defined density interface at the top of the bedload layer (Fig. 7) is needed to form ripples and dunes. In our setting, fine sediments in suspension keep this density profile relatively gentle through the water column (Fig. 7) and delay sediments settling emphasizing the progression of the WESGF. We can thus argue that the high density of the WESGF delays the establishment of a sufficiently well-developed density interface until flow speed reached the lower plane bed stability field skipping dune and ripple fields.

In summary, the physical sedimentary structures described above collectively reinforce the interpretation of our individual facies as sediments deposited within a storm-dominated depositional system.

4.7 - Erosional Surfaces

Erosional surfaces in our studied sections are present only in the lowermost Chicotte Formation capping Facies 1 deposits. Surfaces have up to 10 cm of local relief that truncate grains and cement. In thin section, grains located immediately below this surface show micritic envelopes and early marine, inclusion-rich fibrous to syntaxial cement (Desrochers, 2006).

Several erosional surfaces are present capping meter-scale encrinitic cycles throughout the Chicotte Formation (for detail see Desrochers, 2006). These capping surfaces are relatively simple, planar to low-relief scalloped erosional surfaces, but higher in the Chicotte they are more complex polyphase surfaces formed by distinct, but superimposed erosional events. Truncation of grains along these surfaces implies an early marine cementation to provide a cohesive substrate available for physical erosion at the coastline following a sea level fall.

5 - Facies Assemblages

The nine (9) facies described above and grouped into three (3) FAs represent sediment deposited on a mid to outer carbonate ramp during Telychian time. Our FAs record not only temporal changes in siliciclastic material input (from carbonate dominated FA-3 to mixed carbonate-siliciclastic FA-2 and FA-1), but also spatial changes with more siliciclastic material nearer the basin margin sections (for example in FA-2, Facies 4 is replaced by facies 4a and 6 at Section 1 at the basin margin). Finally, FAs are interpreted to gain a better understanding of their depositional setting.

5.1 - Facies Assemblage 1: Encrinitic Carbonate Facies

Facies Assemblage 1 (FA-1) groups three facies (Facies 1, 2, 3 and minor 7) in the basal Brisante Member of the Chicotte Formation and consists mostly of encrinites or proximal mid-ramp tempestites (Fig. 8). Furthermore, the faunal assemblage (stromatoporoids, platy and colonial tabulate corals and fasciculate rugose corals) in Facies 2 indicates maximum water depths of 20-30 m (Brunton and Copper, 1994), implying a deposition above SWB closer to FWWB. Energy levels are high as supported by the presence of relatively clean encrinitic material. Furthermore, sharp basal contacts and graded encrinite beds suggest sediment reworking and rapid deposition from episodic, high-energy storm events. Fair weather sedimentation was characterized by deposition of suspended fine-grained siliciclastic material, but this material did not have time to accumulate between storm events or was typically reworked by erosion prior to deposition of the next encrinites bed.

In term of facies organization, the FA-1 shows a repetitive meter-scale transgressive-regressive pattern that is well expressed in the field by changes of the weathering profile (Figs. 6 and 9, Plates 1H, 2A); typically thinner- and fining-upward bioturbated encrinites (Facies 3) passing into more thicker- and coarsening-upward clean encrinites (Facies 1). Facies 2 bioherms and biostromes are the only disruption to this pattern and where present occur above Facies 1 and below Facies 3 (9 m above the base of the section, Section 4, Fig. 6). Facies 3 represents sediments that were deposited on a more distal portion of the mid-ramp than Facies 1. Each meter-scale cycle displays lower deepening transgressive (from Facies 1 to Facies 3) and upper shallowing regressive (from Facies 3 to Facies 1) portions. Small bioherms developed locally, but were unable to keep up

with sea level rise and thus gave up. Thus, environmental conditions were too difficult to sustain their growth. Increasing siliciclastic supply was likely an important factor for the deterioration of the reef growth.

5.2 - Facies Assemblage 2: Mixed Siliciclastic and Carbonate Facies

Facies Assemblage 2 (FA-2) groups four carbonate-siliciclastic facies (Facies 4, 5, 6, and 7) present in the uppermost Jupiter Formation (Pavillon Member). FA-2 shows largely bioclastic packstone/grainstone (Facies 4) deposited as distal mid-ramp tempestites, but locally more proximal mid-ramp tempestites are present (Fig. 8). Copper and Long (1990) presented the Pavillon Member with a highly diverse brachiopod fauna probably representing intermediate depth assemblage. Theoretical water depths are provided on Figure 8 inferring deposition up to 60 m deep. HCS and LWR suggest deposition under combined flows in the hummocky zone (Dumas and Arnott, 2006; Dumas et al., 2005; see chapter 4). Bed discontinuity, sharp basal contacts, gutter casts and common graded beds suggest sedimentation from erosive combined to waning flows; the latter evolving into wave enhanced gravity flows in the deeper portion of the ramp. This FA is characterized by a diverse faunal assemblage already dominated by crinoids. Thus, faunal change probably began before the deposition of the Chicotte Formation.

The upper Pavillon succession is organized into two meter-scale packages showing variable amount of Facies 7. Abundant shales and thinner beds, within Facies 4 at specific levels, represent more distal conditions of deposition on a mid-ramp setting. Each meter-scale cycle shows lower deepening transgressive (Facies 4 with increasing amount of Facies 7) and upper shallowing regressive (Facies 4 with decreasing amount of Facies 7) portions. In the basin margin sections (sections 1 and 3), siliciclastic supply was more important allowing deposition of facies 4a and 6. The most likely siliciclastic source is from the north as for the Vauréal Formation with the Precambrian Grenville terrane (Long and Copper, 1987b). The more likely scenario is that siliciclastic sediments came from a delta eastward of the sections, as during the deposition of the Ellis Bay Formation (Farley, 2008), where a mud plume influenced by geostrophic or longshore currents permitted the transport of fine sediments toward the west. Nevertheless, the possibility to have a mud supply crossing the basin from the Appalachians cannot be ruled out as well as fine sediments reworking from the shore during lower energy storms.

Figure 8: Carbonate ramp profile with the spatial distribution of facies. The ramp profile displays here a narrow inner ramp in equilibrium with a high-energy coast line (see section 7.3 for details). Facies are grouped by FA. In FA-1, part of the Facies 7 distribution is striped to represent that no sediment was deposited on the distal mid-ramp in this FA. "P/G" is for "Packstone/Grainstone", "M/W" is for "Mudstone/Wackestone".

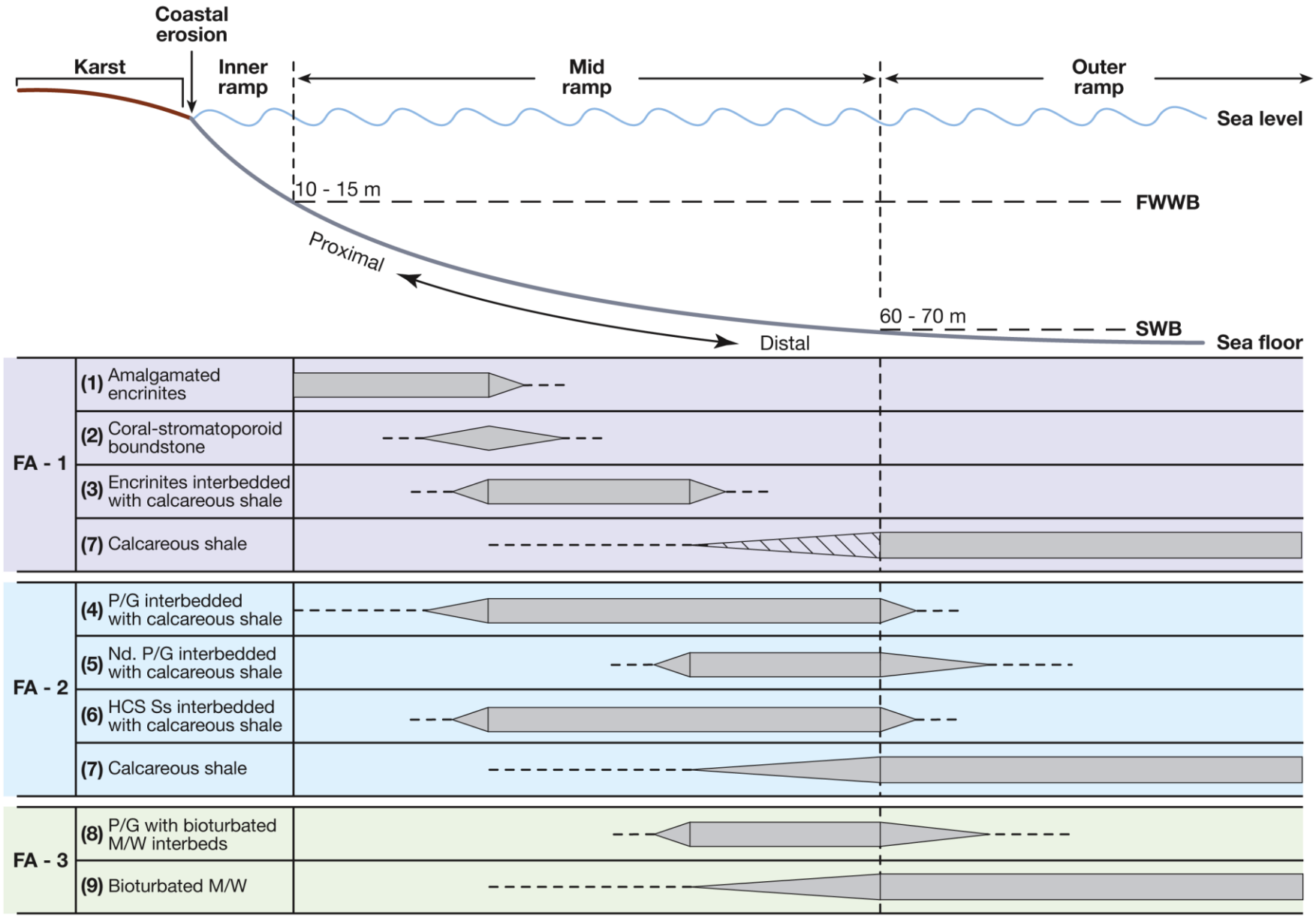
Coastal erosion
Karst
Inner ramp
Mid ramp
Outer ramp
Sea level
10 - 15 m
FWWB
Proximal
60 - 70 m
SWB
Distal
Sea floor
FA - 1
(1) Amalgamated encrinites
(2) Coral-stromatoporoid boundstone
(3) Encrinites interbedded with calcareous shale
(7) Calcareous shale
FA - 2
(4) P/G interbedded with calcareous shale
(5) Nd. P/G interbedded with calcareous shale
(6) HCS Ss interbedded with calcareous shale
(7) Calcareous shale
FA - 3
(8) P/G with bioturbated M/W interbeds
(9) Bioturbated M/W

Figure 9: Stratigraphic facies distribution, TR sequences, sea level fluctuations, climate regime and stable carbon isotope data across the Jupiter-Chicotte formational boundary. The Telychian time slices (*Te1* and *Te2*) are taken from Cramer et al. (2011) and Munnecke and Männik (2009). A sequence stratigraphical frame is proposed displaying two order of sequence: distinct TR meter-scale cycles and a major TR sequence (see section 6 for details). A background frame is also showing the depositional environment (with a gradient from proximal to distal mid-ramp) on the TR sequence succession. Inferred general sea level fluctuations (thick red line) are proposed with smaller frequency variations (thin black line). Climate regime (after Jeppsson, 1990) and stable carbon isotope data (from Munnecke and Männik, 2009) are provided where the point represent measures taken at different stratigraphical levels with error bars and the line the inferred $\delta^{13}C$ variations. Dotted line represents hypothetical $\delta^{13}C$ excursion across the Jupiter-Chicotte formational contact based on Munnecke and Männik (2009).

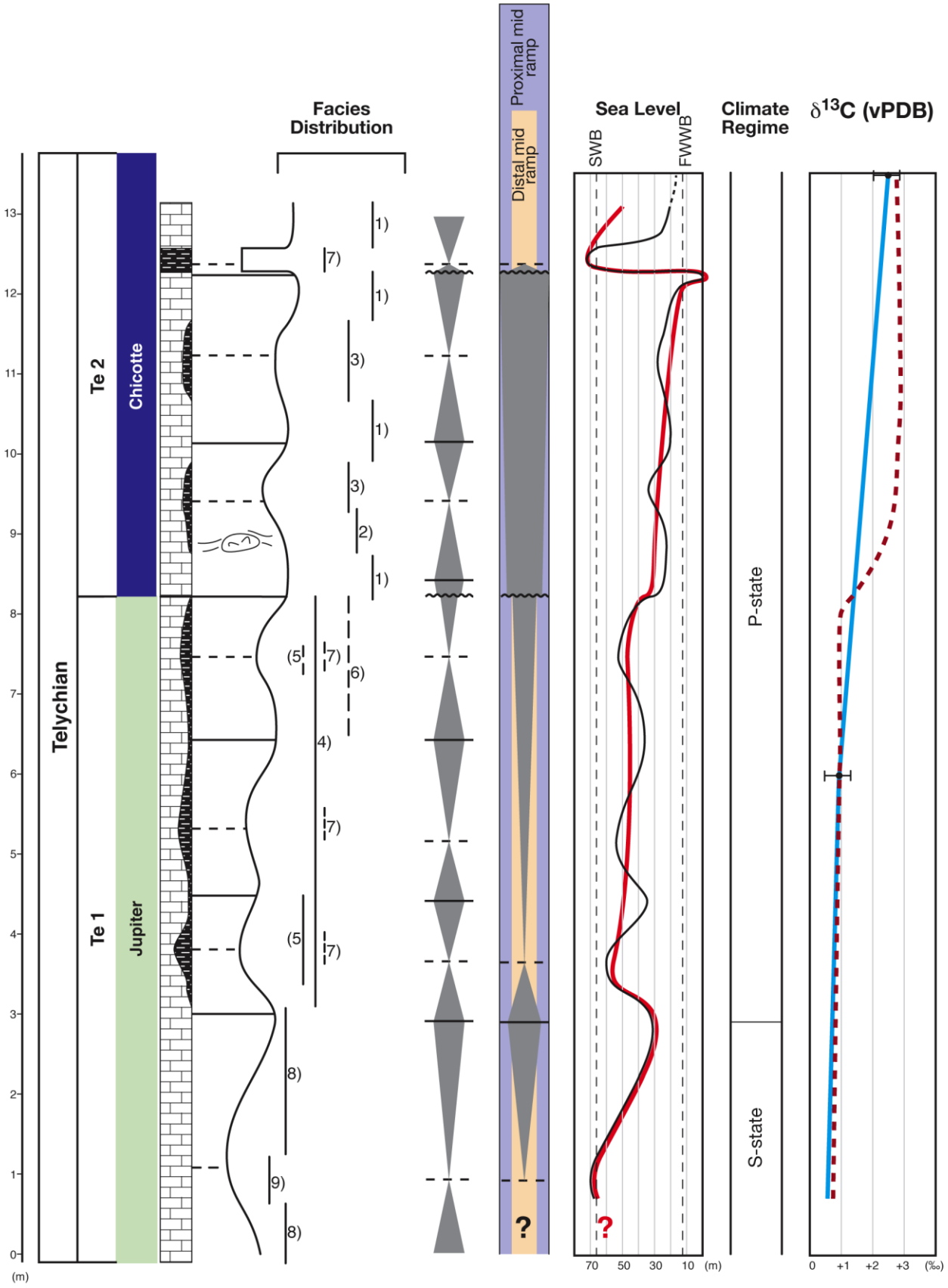
Telychian
Te 2
Te 1
Chicotte
Jupiter
Facies Distribution
Proximal mid ramp
Distal mid ramp
Sea Level
SWB
FWWB
Climate Regime
P-state
S-state
δ13C (vPDB)
(m)
70 50 30 10 (m)
0 +1 +2 +3 (‰)

5.3 - Facies Assemblage 3: Non-Encrinitic Carbonate Facies

Facies Assemblage 3 (FA-3) regroups two carbonate facies (Facies 8 and 9), present at the base of the Pavillon Member at Sections 2 and 4 (Figs. 4 and 6, Plates 1D, 1E, and 1G). FA-3 consists of bioclastic calcarenite/calcirudite (Facies 8) deposited on the distal mid to outer ramp tempestites isolated into bioturbated mudstone/wackestone (Facies 9) representing the fair weather sedimentation (Fig. 8). Tempestites are less abundant and more lenticular than in FA-2. They are interpreted to represent a more distal setting: deposition likely occurred in depths up to 80 m (see Fig. 8). Highly discontinuous, lenticular shaped and commonly graded calcarenites represent wave-enhanced sediment-gravity flow during storms. LWR, present at regular intervals, are the product of combined flows and have a greater preservation potential in more distal mid-ramp setting (Dumas and Arnott, 2006).

The lower Pavillon succession displays one meter-scale cycle composed of Facies 8 and 9 that is well expressed by its weathering profile. Facies 9 is more recessive evidenced by its more intense bioturbation and more abundant lime mud matrix. Facies 9 represents sediments deposited on a more distal mid to outer ramp setting than Facies 8. This meter-scale cycle shows an incomplete lower deepening transgressive portion (Facies 8 changing into Facies 9) and an upper shallowing regressive portion (Facies 9 changing into Facies 8). At the basin margin Section 2, more siliciclastic material was deposited where Facies 8 is locally replaced by Facies 4 (see Figs. 4 and 9).

6 - Sequence Stratigraphy

Sections have been described, according to simple sequence stratigraphic scheme into major transgressive-regressive (TR) sequences and minor meter-scale TR cycles (Embry et al., 2007). This sequence stratigraphy approach is an inductive or data driven approach. Each TR sequence or cycle is delimited by two sequence boundaries (SB), one at its base and one at its top. The SBs are either conformable or unconformable. They typically show an unconformable character at the basin margin and become conformable toward the basin center. They represent the maxima of regression: maximum regressive surface (MRS). MRS separates coarsening upward strata from fining upward strata (Embry, 2001), and a shallowing from a deepening trend. SBs are also defined by a subaerial discontinuity, an unconformable shoreline ravinement surface and occasionally part of a maximum flooding zone (more basinward). The maximum flooding zone (MFZ) marks a change in

trend, within the sequence, from an underlying fining- to an overlying coarsening-upward trend. MFZ delimits deepening- from shallowing-upward packages called respectively transgressive system tract (TST) and regressive system tract (RST). TST is composed by all the strata deposited during transgression. RST is composed by all the strata deposited during regression. If enough information is available, we can distinguish an early (ERST) and late regressive system tracts (LRST). ERST and LRST, respectively, correspond to highstand and lowstand system tracts of Posamentier and Allen (1999). Their contact can be sharp or gradational, conformable or unconformable. On the field, the regressive trend is obvious through the two RSTs, but the LRST shows a major facies offset. Two orders of stratigraphic units are present in this study; one complete TR sequence with five (5) meter-scale cycles (Fig. 9).

6.1 - TR Sequence

A major TR sequence comprises the uppermost five (5) meters of the Pavillon Member and the four lowermost meters in the Brisante Member (Fig. 9). Its lower SB is placed at the top of a shallowing-upward package in the lower Pavillon Member (3 meters above the base of Section 4, Fig. 9) and corresponds to a MRS (present in sections 2 and 4). The TST comprises only the first meter where shale interbeds are present. The RST, better developed than the TST, ends at the top of the first coarse-grained encrinitic package in the Chicotte Formation. The RST is completely exposed at Section 4, but partially missing at the other sections. The RST is marked by a facies offset along a distinct sharp-based surface (also the Jupiter-Chicotte formational boundary) separating an ERST from a LRST. Facies across this surface show an abrupt shift in depositional facies from distal mid-ramp to proximal mid-ramp deposits. The upper SB is a MRS characterized by the presence of an erosional surface recording subaerial exposure and physical coastal erosion (Desrochers, 2006).

6.2 - TR Meter-Scale Cycles

Five (5) TR meter-scale cycles are present (see Fig. 9). The thickness of the cycle varies from 1 to 3 meters. The TST is typically less developed than the RST within an individual cycle. The cycles display a prograding stacking pattern developed under the influence of a long-term base level fall.

7 - Discussion

7.1 - Regional Correlations

The Jupiter-Chicotte formational contact is well defined in the southwestern part of Anticosti Island, but it is difficult to recognize this formation further east where small patches of Chicotte encrinites have been previously mapped (Bolton, 1972; Petryk, 1981; Copper and Long, 1990). In our study, the easternmost sections 1 and 3 were mapped as Chicotte Formation. This is unlikely based on lithological, stratigraphical and paleontological evidences (Fig. 10).

The Jupiter-Chicotte contact is best defined at Section 4 where more resistant Facies 1 beds are abruptly overlying the more recessive Facies 4. A similar facies change with its distinct weathering profile is not seen at the top of Section 3 where some crinoid-rich grainstones are present. At Section 1, a similar weathering profile is present, but lithologies are mainly Facies 4 packstones/grainstones and not encrinites. In addition Facies 4 shows, at Section 1, an amalgamated character interpreted as proximal tempestites with a coarser siliciclastic supply (Facies 4a). This siliciclastic supply has been recognized further west in Section 3. As typical Chicotte facies (i.e. Facies 1 to 3) are, here, absent we conclude that the uppermost part of Section 1 is likely in the Jupiter Formation.

Our main TR sequence is tentatively correlated at the four studied locations (Fig. 10). Its lower SB is recognized at sections 2 and 4, separating FA-3 and FA-2. The MFZ is in the basal first meters (at sections 2 and 4) but the upper SB is only observed at Section 4 within the basal Chicotte Formation. Our correlation is supported by sequence stratigraphic principles and the overall spatial facies distribution: FA-3 is only present below the TR sequence whereas FA-2 represents most of the sequence along the studied outcrop belt. FA-1 is present in the LRST of the main TR sequence in Section 4. Within the main TR sequence, the correlation of meter-scale cycles is more coherent with our interpretation and explains the presence of coarser siliciclastic material mixed with carbonate lithologies at the east end of our outcrop belt. Further works, especially more detailed mapping along the southeastern coast of the island is needed to confirm the general absence of Chicotte strata at the east end.

7.2 - Sediment Dynamics

Based on our facies interpretation, the Anticosti depositional ramp was under a sedimentary regime dominated by storms, not only during the deposition of the Jupiter and Chicotte formations but also during the entire Llandovery (Long, 2007; Sami and Desrochers, 1992). Thus sedimentation rates probably did not change throughout the Early Silurian. The rate of accommodation space was most likely controlled by tectonic subsidence and sea level changes.

7.2.1 - Evidence for Tectonic Subsidence

Unlike the interior of the North American craton, Anticosti Island presents one of the most complete sections of the Ordovician-Silurian boundary in North America (Barnes, 1988). Its Llandovery succession is represented at least by 500 m of strata. The upper Chicotte boundary is not well biostratigraphically constrained, thus, this thickness of 500 m should be considered as a minimum thickness for the Llandovery present on Anticosti Island. On the other hand, Llandovery successions exceed rarely 200 m in North America (Mikulic, 1991). In the Appalachian Basin, at least six regional unconformities subdivide the Lower Silurian succession (Brett et al., 1990). Anticosti Island, as part of the Appalachian foreland basin, underwent tectonic subsidence under the influence of Taconian and Early Acadian Orogenies (see Fig. 2). The progression of the Taconian deformation front, southward of Anticosti, provided sufficient load to allow the whole Anticosti Platform to subside. According to Long (2007), tectonic subsidence rates increased (up to 17.87 cm/ky) in the Late Ordovician with the Taconic Event, but then decreased in the Llandovery, to around 1 cm/ky on average. Rates of 0.2 cm/ka were calculated for the upper Jupiter and Chicotte Formations. Pinet (2011) related some deformation events south of the St Lawrence Platform to an Aeronian punctual increase in tectonic subsidence rates. Thus, the upper Jupiter and Chicotte Formations (Telychian) are characterized by slower tectonic subsidence after higher rates identified in the Gun River and lower Jupiter formations (Aeronian). Nonetheless, Telychian tectonic subsidence rates can be underestimated because of the lack of well-constrained ages for the uppermost Chicotte Formation (Long, 2007) and several erosional breaks present within the Chicotte Formation (Desrochers, 2006). On the other hand, the Taconian orogeny is believed to be active especially in the St Lawrence promontory during the Early Silurian (Ettensohn and Brett, 2002). Even if it has been argued that the biostratigraphy does not allow precisely dating of this tectonic pulse, we believe that given the sedimentation rates, changes in tectonic subsidence did not trigger the stratigraphical changes in our sections. Nevertheless, tectonic subsidence can explain the

Figure 10: E-W correlation of our main TR sequence and m-scale cycles. The TR sequence is represented on the right; five distinct m-scale cycles have been recognized from which three are numerated from A to C for correlation. See text for details.

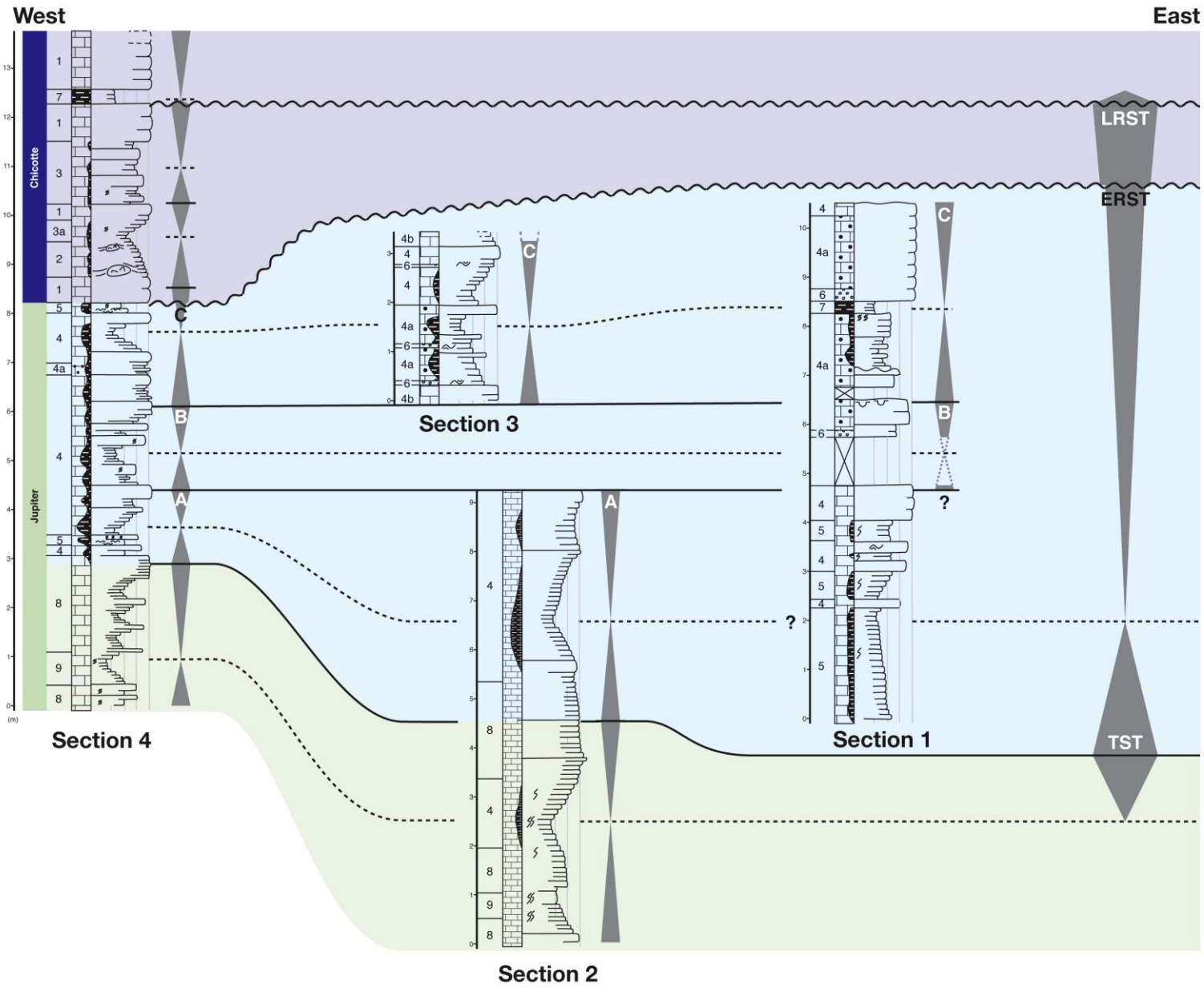
West
East
Chicotte
Jupiter
LRST
ERST
TST
A
B
C
?
Section 1
Section 2
Section 3
Section 4

difference in thickness that was observed though the outcrop belt (Fig. 10), as well as eventual siliciclastic mud supply pulses across the basin.

7.2.2 - Evidence for Sea Level Change

Sea-level changes are well expressed in our sections as illustrated by lithological, sedimentological and stratigraphical trends. They show rapid facies changes often corresponding to an important temporal and spatial shift of the depositional environments along the Anticosti ramp. The only process able to generate sea-level changes with such high frequencies (tens to hundreds of thousands of years) and significant amplitudes (several tens of meters) is glacio-eustacy. Thus, fluctuations of continental ice-sheets can significantly influence the eustatic signal. Evidence for Early Silurian glaciations is present during the Llandovery (Diaz-Martinez and Grahn, 2007). An early Telychian glacial episode is well known from South America (Grahn and Caputo, 1992; Caputo, 1998). As we mentioned above, the upper Jupiter and lower Chicotte formations are LowerTelychian in age. According to Long's calculations (2007, Table 1), our 13 m thick Early Telychian section represents approximately a 0.5 to 1.0 My long time interval. Our main TR sequence is interpreted to represent a ~0.4 My time interval while meter-scale TR cycles around ~0.1 My. Thus, the main TR sequence is likely 4^{th} order in scale and represents probably eccentricity related orbital periodicities. Smaller scale cycles (1-3 m thick) are likely 5^{th}-6^{th} order in scale and represent probably short eccentricity and/or obliquity orbital periodicities. The overall shallowing trend present in the upper Jupiter and Chicotte strata is consequently part of a longer-term 3^{rd} order sea level fall in scale linked to either the decreasing rate of tectonic subsidence and/or a more global long-term eustatic signal.

7.2.3 - Evidence for Climate or Nutrient Supply Change

The Silurian has long been considered as a greenhouse interval but Early Silurian glaciations are now known (Grahn and Caputo, 1992; Caputo, 1998; Diaz-Martinez and Grahn, 2007; Le Heron et al., 2009; Munnecke et al., 2010). An icehouse period is now defined from the Katian to the Llandovery and known as the "Early Paleozoic Icehouse" (Page et al., 2007). As mentioned above, the relatively important and frequent sea level changes recorded in our studied strata most probably represent fluctuations of ice sheet volume. In addition, we observed a distinct lithological change in our studied sections with an abrupt increasing upward siliciclastic content.

This drastic change from a carbonate to mixed siliciclastic-carbonate depositional regime suggests a change in weathering rates and sediment supply from the adjacent continental landmass, a few tens of kilometers to the North. As it has been shown, siliciclastic sands are brought from the north shore, it is not necessarily the case for siliciclastic mud. More weathering implies a more humid climate. This change can be integrated into Jeppsson's (1990) climatic model for the Silurian. The lower part of the Pavillon Member correlates well with the Secundo State characterized by a carbonate regime under arid conditions at low latitudes (low rate of weathering). On the other hand, the upper part of the Pavillon Member and basal Chicotte beds (and possibly the rest of the latter formation) relates to the Primo State and mixed siliciclastic-carbonate facies under humid conditions (high rate of weathering). This is counterintuitive with respect to more recent icehouse periods when climates were dryer at a global scale (Ruddiman, 2008). Nevertheless, our local study shows more humid conditions during a glacial episode as suggested by the increasing amount of siliciclastics on the Anticosti ramp at that time. An alternative interpretation involves a major temporal shift in the supply of siliciclastic material from a distant deltaic source, but at this stage we do not know if the siliciclastic material was supplied to the ramp from a major point source or from a multi-entry linear source. This siliciclastic supply was, however, sustained over a long period unlike the rapid spatial lobe switch observed in modern deltas; like for the modern Mississippi delta.

Increasing siliciclastic supply provided a good source of nutrients for filter-feeder organisms like crinoids. This sudden increase in nutrients can play an important role in the benthic ecosystem with the domination by crinoids. However, crinoid domination post-dated the pulse of siliciclastic that is recorded in the upper part of the Pavillon Member. We argue, therefore, that this change did not trigger ecosystem reorganization on the Anticosti ramp (see section 7.4).

7.2.4 - Evidence for Sea Water Chemistry Change

Stable carbon isotope data from Anticosti Island show "a small but distinct positive excursion of $\delta^{13}C$, with peak values of 3.2‰ VPDB in the lowermost 10-15 m of the Chicotte Formation" (Munnecke and Männik, 2009; see Fig. 9). When compared to other positive carbon isotope excursions present throughout the Ordovician and Silurian, I observed similar lithological, paleontological and geochemical characteristics (Munnecke et al., 2003). Thus, "similar environmental changes are likely responsible" implying a "common steering mechanism"

(Munnecke and Männik, 2009). A definitive mechanism has not yet been proposed to explain this change in the global carbon cycle, but several hypotheses have been proposed.

Kump and Arthur (1999) proposed a decrease in silicates weathering as a cause but this is highly unlikely due to increased in weathering recorded in strata of the uppermost Jupiter Formation. Bickert et al. (1997) proposed a similar explanation with their climatic model in which high $\delta^{13}C$ is recorded during periods of aridity. In our case, sediments deposited at or near the excursion are characterized by more humid conditions (i.e. Jeppsson's P-state).

Wenzel and Joachimski (1996) suggested a productivity hypothesis implying two states. At high sea level state, warm saline deep water causes an oxygen deficiency in the basin. This sluggish circulation results in reduced primary productivity and thus low $\delta^{13}C$ values. At low sea level state, on the other hand, high $\delta^{13}C$ values are explained by upwelling circulation. It provides nutrients to surface waters stimulating primary productivity. The model fits with the $\delta^{13}C$ data: in the Jupiter Formation, $\delta^{13}C$ shows values around 1‰ VPDB whereas in the Chicotte Formation, at lower sea level, values are close to 3‰ VPDB (Munnecke and Männik, 2009). Nevertheless, the Anticosti Platform was part of a foreland basin developed during the partial closure of the Iapetus Ocean (Long, 2007). We believe that the basin was relatively closed with limited connection to the open ocean. It is consequently difficult to explain this carbon excursion recorded on Anticosti in link with global ocean circulation. On the other hand, a similar geochemical event in age was recorded on Baltica coinciding with a distinct conodont extinction event, called the Valgu event, and supporting a weak primary productivity (Munnecke and Männik, 2009).

The weathering hypothesis from Kump et al. (1999) remains the only other plausible explanation to explain such positive carbonate isotope excursion. Their model was originally proposed to explain the positive 6‰ $\delta^{13}C$ Hirnantian excursion. The model considers the isotopic signature of the riverine influx and the rate of weathering of subaerially exposed carbonates in order to produce a positive isotopic excursion. The positive 2‰ $\delta^{13}C$ excursion recorded in the basal Chicotte Formation could be explained by such mechanism, but operating on a smaller scale than the Hirnantian glacial maximum. In our case, the extension of this isotopic excursion higher into the Chicotte Formation toward a major intraformational discontinuity (Desrochers, 2006) is not yet documented. A more complex, but possible mechanism could combine the effects of some of these previous models (high nutrients fertile surface waters versus high weathering under more humid conditions) in order to control various $\delta^{13}C$ source and drive a positive carbon isotope excursion.

7.3 - Carbonate Ramp Model

In a classic paper, Burchette and Wright (1992) examined carbonate ramp depositional systems and divided a typical carbonate ramp into an inner, a mid and an outer segments. Their inner ramp segment is characterized by facies above FWWB including shoreface, beach, lagoon or tidal flat. Jones (2010) presented recently a similar ramp model with a wide inner ramp segment. As the eastern margin of Laurentia was covered by shallow epeiric seas during most of the Early Silurian (Long, 2007), we should find evidence for intertidal and supratidal facies. Early Paleozoic peritidal environments are notably characterized by m-scale shallowing-upward sequences ranging from subtidal to supratidal facies (Pratt et al., 1994). As a modern ramp example, Jones (2010) described the Persian Gulf where mixed siliciclastic-carbonate sediments are accumulating today in an asymmetric foreland basin winnowed by strong seasonal winds. This example is the closest analog to our Late Ordovician-Early Silurian Anticosti ramp, but the former shows extensive development of sabkha, intertidal microbial flats, and lagoonal environments. These distinct peritidal sediments are conspicuously absent in our studied succession. We proposed that peritidal sediments in our succession, if present at all, had little or no chance to be preserved in the rock record because its peculiar sediment dynamics dominated by rapid sea level changes (see above section), but also by an overall ramp geometry controlled by wave energy conditions.

The proposed model is closer to a siliciclastic wave-dominated ramp than a typical gently sloping carbonate ramp (Fig. 8). A wave-dominated shoreface shows typically a concave-up profile, with a steep proximal part. The break in the slope occurs at depth of about 10 m (close to FWWB). Unlike the more classic carbonate ramp model with an uniform slope (< 1°), our proposed ramp shows a relatively narrow, inner ramp (only a few km wide) where the slope is the steepest. Mid and outer ramp segments are wider (tens to hundreds of km) as the slope is gentle again. Coastal erosion occurred at the shoreline forming the subtle erosional surfaces present in the lower part of the Chicotte Formation, but also high relief rocky shorelines present higher in the same formation (Desrochers, 2006). A narrow shoreline sediment wedge adjacent to these shorelines was locally preserved filling associated paleotopographic depressions. As we know, on the shoreface, fair weather conditions tend to transport sediment onshore whereas storms carry sediment seaward (Clifton, 2006). In his idealized diagram, Clifton (2006) assumed that only coarser-grained sediments are left after storm and fair weather conditions, thus, providing a key feature to recognize lower shoreface from inner shelf sediments. Typical bimodal sediment is left over on the shoreface. In our case, we probably do not have enough fine sand supply to preserve the finer fraction, but gravels can

be preserved. Nonetheless, Clifton (2006) considered siliciclastic gravels, which are denser than carbonates gravels. Thus, we should preserve even coarser material in our inner ramp sediments: like brachiopod shells and crinoidal calcarenites (Desrochers, 2006). Not much sediment is left as deposited in the shoreface. We thus assume that frequent storm activity keeps the shoreface steep and relatively sediment free. This could prevent the traditional low-energy muddy peritidal environments to develop. In addition, coastal erosion decreases the potential to preserve such peritidal facies when the shoreline is constantly responding to relative sea level changes.

7.4 - Change in Benthic Communities: Domination of Crinoids

The early Paleozoic crinoids reached their peak in diversity during the Telychian and were abundant in both shallow and deep shelf environments (Ausich and Copper, 2010). In our studied sections, crinoids are more common in the siliciclastic-rich FA-2, but their dominance started only with the deposition of FA-1 at the base of the Chicotte Formation.

Optimal conditions for the development of crinoid banks appeared in the upper Pavillon Member, as nutrients were brought with the increasing siliciclastic supply and settled in a relatively quiet environment (except during storms). Therefore, another factor must have played an important role for their extensive development in the basal Chicotte Formation. The Jupiter-Chicotte formational boundary records an important change in depositional environments triggered by a forced sea level fall. This could have introduced more advantageous conditions for crinoids over the other benthic taxa. Furthermore, numerous hardgrounds are present at the base of the Chicotte Formation. These hardgrounds represent extensive sea floor cementation and change in the nature of the substrate requiring a new life strategy from the benthic communities. These conditions were optimal for crinoids taking advantage of this new environment. This initial development was, however, sustained by a longer-term feedback mechanism. The Chicotte crinoids produced coarse-grained sediment substrates following either their post-mortem disintegration or their rapid transportation and deposition following a storm event. They had well adapted root systems able to recolonize quickly these gravel substrates. With sufficient nutrient supply, sustained storm activity and repetitive substrate changes, crinoids were able to colonize the entire ramp and dominate benthic communities.

8 - Conclusions

The study of the Lower Silurian succession at the Jupiter-Chicotte formational boundary on Anticosti Island led to the identification of nine facies grouped into three facies associations (FA-1 to FA-3). These facies were largely deposited on a mixed siliciclastic-carbonate, storm-dominated ramp. The main conclusions of this facies analysis can be summarized as follows:

- Spatial and temporal changes in the siliciclastic content allow us to identify more siliciclastic-rich depositional environments in the eastern basin margin sections, and a climatic change in time from arid to more humid conditions.
- One TR sequence and several meter-scale TR cycles are recognized in our four studied sections allowing us to improve the existing E-W lithological correlations.
- The rate of sediment accommodation on the Anticosti ramp was mainly driven by various orders of sea level fluctuations during the Telychian, as tectonic subsidence rates were progressively decreasing following a brief pulse during the Aeronian.
- The TR sequence and meter-scale cycles recorded high frequency glacio-eustatic fluctuations forced by a glacial episode present over the South American Gondwana during the early Telychian. The main TR sequence is likely to be 4^{th} order (~400 Ky) whereas meter-scale cycles are 5^{th} and/or 6^{th} order (~100 Ky).
- Our depositional ramp model shows a concave-up profile departing from the classic gently sloping profile and is characterized by a narrow, steep inner ramp in equilibrium with high wave energy conditions.
- The predominant benthic communities shifted in time from brachiopods to crinoids during the Early Telychian in response to increasing siliciclastic supply, rapid sea level fluctuations and early marine (?) cemented gravel substrates.

Finally, further work is needed to clarify some issues addressed in this study including: 1) additional mapping and section description at the basin margin to improve our E-W correlations; 2) more detailed geochemical analysis on the major and minor element composition of the Jupiter-Chicotte shales to constrain environmental parameters in the basin and sediment provenance; and 3) additional stable isotopic analysis to place more accurately the stratigraphic extension of the positive carbon isotope excursion within the Chicotte Formation.

References

ARNOTT, R.W.C., *in press*. Turbidites, and the Case of the Missing Dunes. Journal of Sedimentary Research.

AUSICH, W.I., 1997. Regional Encrinites: a vanished lithofacies. *In* Paleontological events, stratigraphic, ecological and evolutionary implications, *edited by* C.E. Brett and G.C. Baird. Columbia University Press, New York, p. 509-520.

AUSICH, W.I., and Copper, P., 2010. The Crinoidea of Anticosti Island, Québec (Late Ordovician to Early Silurian). Palaeontographica canadiana, No. 29.

AZMY, K., Veizer, J., Bassett, M.G., and Copper, P., 1998. Oxygen and carbon isotopic composition of Silurian brachiopods: implications for coeval seawater and glaciations. GSA Bulletin 110, p. 1499-1512.

BARNES, C.R., 1988. Stratigraphy and paleontology of the Ordovician-Silurian boundary interval, Anticosti Island, Québec, Canada. Bulletin British Museum Natural History (Geology), Vol. 43, p. 195-219.

BARNES, C.R., 1989. Lower Silurian chronostratigraphy of Anticosti Island, Québec. *In* A Global Standard for the Silurian System, *edited by* C.H. Holland and M.G. Basset. National Museum of Wales, Geological Series 9, p. 101-108.

BICKERT, T., Pätzold, J., Samtleben, C., and Munnecke, A., 1997. Paleoenvironmental changes in the Silurian indicated by stable isotopes in brachiopod shells from Gotland, Sweden. Geochimica et Cosmochimica Acta 61, p. 2717–2730.

BOLTON, T.E., 1972. Geological map and notes on the Ordovician and Silurian litho- and biostratigraphy, Anticosti Island, Québec. Geological Survey of Canada, Paper 71-19.

BORDET, E., Malo, M., and Kirkwood, D., 2010. A structural study of Western Anticosti Island, St. Lawrence Platform, Québec: a fracture analysis that integrates surface and subsurface structural data. Bulletin of Canadian Petroleum Geology, Vol. 58, No. 1, p. 36-55.

BRETT, C.E., Goodman W.M., and LoDuca S.T., 1990. Sequences, cycles, and basin dynamics in the Silurian of the Appalachian Foreland Basin. Sedimentary Geology, Vol. 69, p. 191-244.

BROOKFIELD, M.E., and Silvestro, S., 2010. Eolian systems. *In* Facies Models 4, *edited by* N.P. James and R.W. Dalrymphe, Geological Association of Canada, p. 139-166.

BRUNTON, F.R., (1988a). Silurian (Llandovery-Wenlock) patch reef complexes of the Chicotte Formation, Anticosti Island, Québec. M.Sc. Thesis, Laurentian University, Sudbury, Ontario.

BRUNTON, F.R., and Copper P., 1994, Paleoecologic, temporal, and spatial analysis of Early Silurian reefs of the Chicotte Formation, Anticosti Island, Québec, Canada. Facies, Vol. 31, p. 57-80.

BURCHETTE, T.P., and Wright, V.P., 1992. Carbonate ramp depositional systems. Sedimentary Geology, Vol. 79, p. 3-57.

CAPUTO, M.V., 1998. Ordovician-Silurian glaciations and global sea-level changes. *In* Silurian Cycles; Linkages of Dynamic Stratigraphy with Atmospheric, Oceanic, and Tectonic Changes, *edited by* E. Landing, M.E. Johnson. New York State Museum Bulletin 491, p. 15-25.

CHEN, H.B., Hilko, B., and Panarella, E., 1994. The Rayleigh-Taylor Instability in the spherical pinch. Journal of Fusion Energy, Vol. 13, p. 275-280.

CLIFTON, H.E., 2006. A re-examination of Facies Models for clastic shorelines. *In* Facies Models Revisited, *edited by* H.W. Posamentier and R.G. Walker. SEPM Special Publication 84, p. 293-337.

COPPER, P., 1981. Atrypoid brachiopods and their distribution in the Ordovician-Silurian Sequence of Anticosti Island. *In* P.J. Lespérance (editor) I.U.G.S. Field Meeting, Anticosti-Gaspé, Québec,

1981. Volume II Stratigraphy and Paleontology. Département de Géologie, Université de Montréal, p. 137-142.

COPPER, P., and Long, D.G.F., 1990. Stratigraphic revision of the Jupiter Formation, Anticosti Island, Canada; a major reference section above the Ordovician-Silurian Boundary. Newsletters on Stratigraphy, Vol. 23(1), p. 11-36.

COPPER, P., and Jin, J., 1995. Field guide to Ordovician-Silurian brachiopods of Anticosti Island, Eastern Canada. 3rd International Brachiopod Congress, 25-30 August 1995, 28 p.

COPPER, P., 1997. Two successive Ordovician/Siluriamn mass extinction boundary events on Anticosti Island, Eastern Canada, within 1 My. Geological Society of America Annual Meeting, Abstracts, Salt Lake City, October 20-23, 1997, 1 p.

COPPER, P., and Long, D.G.F., 1998. Part 2: Sedimentology and paleontology of the Late Ordovician through Early Silurian shallow water carbonates and reefs of the Anticosti Island, Québec. *In* GAC/MAC/CGU Joint Annual Meeting, Québec City, Québec, Canada, Field Trip B8 Guidebook, p. 55-94.

CRAMER, B.D., Brett, C.E., Melchin, M.J., Männik, P., Kleffner, M.A., McLaughlin, P.I., Loydell, D.K., Munnecke, A., Jeppsson, J., Corradini, C., Brunton, F.R., and Saltzman, M.R., 2011. Revised correlation of Silurian provincial series of North America with global and regional chronostratigraphic units and $\delta^{13}C_{carb}$ chemostratigraphy. Lethaia, Vol. 44, p. 185-202.

CUMMINGS, D.I., Dumas, S., and Dalrymple R.W., 2009. Fine-grained versus coarse-grained wave ripples generated experimentally under large-scale oscillatory flow. Journal of Sedimentary Research, Vol. 79, p. 83-93.

DESROCHERS, A., 2004. High frequency sea-level fluctuations in encrinite and reefal limestones accumulating along rocky shorelines: an example from the Lower Silurian Chicotte Formation, Anticosti Island, Canada. *In* Proceedings of the 32nd International Geological Congress, Florence, Italy, 20-28 August 2004. IGC Secretariat, Firenze, Italy.

DESROCHERS, A., 2006. Rocky shoreline deposits in the Lower Silurian (Upper Llandovery, Telychian) Chicotte Formation, Anticosti Island, Québec. Canadian Journal of Earth Sciences 43, p. 1205–1214.

DESROCHERS, A., Bourque, P.-A., and Neuweiler, F., 2007. Diagenetic versus biotic accretionary mechanisms of bryozoan-sponge buildups (Lower Silurian, Anticosti Island, Canada). Journal of Sedimentary Research, Vol. 77, p. 564-571.

DESROCHERS, A., and Gauthier, E.L., 2009. Carte géologique de l'Île d'Anticosti (1/250 000). Ministère des Ressources Naturelles et de la Faune du Québec, DV 2009-03.

DESROCHERS, A., Farley, C., Achab, A., Asselin, E., and Riva, J.F., 2010. A far-field record of the End Ordovician Glaciation: the Ellis Bay Formation, Anticosti Island, Eastern Canada. Palaeogeography, Palaeoclimatology, Palaeoecology 296, p. 248-263.

DEWING, K., 1999. Late Ordovician and Early Silurian strophomenid brachiopods of Anticosti Island, Québec, Canada. Palaeontographica Canadiana No.17, p. 1-143.

DIAZ-MARTINEZ, E., and Grahn, Y., 2007. Early Silurian glaciation along the western margin of Gondwana (Peru, Bolivia and northern Argentina): Palaeogeographic and Geodynamic Setting. Palaeogeography, Palaeoclimatology, Palaeoecology 245, p. 62-81.

DICKSON, J.A., 1966. Carbonate identification and genesis as revealed by staining. Journal of Sedimentary Petrology, Vol. 36(2), p. 491-505.

DOTT, R.H.Jr, 1983. Episodic sedimentation – How normal is average? How rare is rare? Does it matter? Journal of Sedimentary Petrology, Vol. 53, p. 5-23.

DUMAS, S., Arnott, R.W.C., and Southard, J.B., 2005. Experiments on oscillatory-flow and combined flow bed forms: implications for interpreting parts of the shallow marine rock record. Journal of Sedimentary Research, Vol. 75, No. 3, p. 501-513.

DUMAS, S., and Arnott, R.W.C., 2006. Origin of hummocky and swaley cross-stratification – The controlling influence of unidirectional current strength and aggradation rate. Geology, Vol. 34, No. 12, p. 1073-1076.

DUNHAM, R.J., 1962. Classification of carbonate rocks according to depositional texture. *In* Classification of carbonate rocks, *edited by* W.E. Ham. AAPG Memoir 1, p. 108-121.

EMBRY, A.F., and Klovan, J.E., 1971. A Late Devonian reef tract on northeastern Bank Island. Canadian Petroleum Geology Bulletin, Vol. 19, p. 730-781.

EMBRY, A., 2001. The six surfaces of sequence stratigraphy. AAPG Hedberg Conference on sequence stratigraphic and allostratigraphic principles and concepts, Dallas. Abstract volume, p. 26-27.

EMBRY, A., Johannessen, E., Owen, D., Beauchamp, B., and Gianolla, P., 2007. Sequence Stratigraphy as a "concrete" stratigraphic discipline. Report of the ISSC Task Group on Sequence Stratigraphy, p. 1-104.

ETTENSOHN, F.R., Brett, C.E., 2002. Stratigraphic Evidence from the Appalachian Basin for Continuation of the Taconian Orogeny into the Early Silurian Time. Physiscs and Chemistry of the Earth 27, p. 279-288.

FARLEY, C., 2008. Sediment Dynamics and Stratigraphic Architecture of a Mixed Carbonate-Siliciclastic Ramp: The Upper Ordovician (Hirnantian) Ellis Bay Formation, Anticosti Island, Québec, Canada. M.Sc. Thesis, University of Ottawa, Ottawa, Ontario.

FRIEDICHS, C.T., and Wright, L.D., 2004. Gravity-Driven Sediment Transport on the Continental Shelf: Implications for Equilibrium Profiles near River mouths. Coastal Engineering, Vol. 51, p. 795-811.

GRABAU, A.W., 1904. On the classification of sedimentary rocks. American Geologist, Vol. 33, p. 228-247.

GRAHN, Y., and Caputo, M.V., 1992. Early Silurian glaciations in Brazil. Palaeogeography, Palaeoclimatology, Palaeoecology 99, p. 9-15.

HEROUX, N.P., Hubert, C., Mamet, B., and Roux, A., 1977. Algues Siluriennes de la Formation de Sayabec (Lac Matapédia, Québec). Canadian Journal of Earth Sciences, Vol. 14, p. 2865-2908.

JAMES, N.P., and Wood, R., 2010. Reefs. *In* Facies Models 4, *edited by* N.P. James and R.W. Dalrymphe, Geological Association of Canada, p. 421-447.

JEPPSSON, L., 1990. An oceanic model for lithological and faunal changes tested on the Silurian record. Journal of the Geological Society, London 147, p. 663-674.

JIN, J., and Copper, P., 1998. *Kulumbella* and *Microcardinalia* (*Chiastodoca*) new subgenus, Early Silurian divaricate stricklandiid brachiopods from Anticosti Island, Eastern Canada. Journal of Paleontology, Vol. 72, p. 441-453.

JIN, J., and Copper, P., 2000. Late Ordovician and Early Silurian pentamerid brachiopods from Anticosti Island, Québec, Canada. Paleontographica Canadiana, Vol. 18, p. 1-140.

JIN, J., 2008. Environmental control on temporal and spatial differentiation of Early Silurian pentamerid brachiopod communities, Anticosti Island, Eastern Canada. Canadian Journal of Earth Sciences, Vol. 45, p. 159-187.

JONES, B., 2010. Warm-water neritic carbonates. *In* Facies Models 4, *edited by* N.P. James and R.W. Dalrymphe, Geological Association of Canada, p. 341-369.

KUMP, L.R., and Arthur, M.A., 1999. Interpreting carbon-isotope excursions: carbonates and organic matter. Chemical Geology 161, p. 181-198.

KUMP, L.R., Arthur, M.A., Patzkowsky, M.E., Gibbs, M.T., Pinkus, D.S., and Sheehan, P.M., 1999. A weathering hypothesis for glaciation at high atmospheric pCO_2 during the Late Ordovician. Palaeogeography, Palaeoclimatology, Palaeoecology 152, p. 173-187.

LAVOIE, D., 2008. Appalachian foreland basins of Canada. *In* Sedimentary Basins of the United States and Canada, *edited by* A.D. Miall. Elsevier Science, Sedimentary basins of the World, Vol. 5, p. 66-103.

LE HERON, D.P., Craig, J., and Etienne, J.L., 2009. Ancient glaciations and hydrocarbon accumulations in Middle East. Earth-Science Reviews 93, p. 47-76.

LONG, D.G.F., and Copper, P., 1987b. Late Ordovician Sand-Wave Complexes on Anticosti Island, Québec: A Marine Tidal Embayment? Canadian Journal of Earth Sciences, Vol. 24, p. 1807-1832.

LONG, D.G.F., and Copper, P., 1994. The Late Ordovician – Early Silurian carbonate tract of Anticosti Island, Gulf of St. Lawrence, Eastern Canada. Field Trip Guidebook B4, Geological Association of Canada and Mineralogical Association of Canada Joint Annual Meeting, Waterloo, Ontario.

LONG, D.G.F., 2007. Tempestite frequency curves: a key to Late Ordovician and Early Silurian subsidence, sea-level change, and orbital forcing in the Anticosti Foreland Basin, Québec, Canada. Canadian Journal of Earth Sciences, Vol. 44, p. 413-431.

MACQUAKER, J.H.S., Bentley, S.J., Bohacs, K.M., 2010. Wave-Enhanced Sediment-Gravity Flows and Mud Dispersal across Continental Shelves: Reappraising Sediment Transport Processes Operating in Ancient Mudstone Successions. Geology, Vol. 38, p. 947-950.

MAMET, B., Roux, A., Lapointe, M., and Gauthier, L., 1992. Algues Ordoviciennes et Siluriennes de l'Île d'Anticosti (Québec, Canada).Revue de Micropaléontologie, Vol. 35, n° 3, p. 211-248.

MIKULIC, D.G., 1991. Tippecanoe II Subsequence - Silurian system through Lower Devonian Series. *In* Interior cratonic basins, *edited by* M.W. Leighton, D.R. Kolata, D.F. Oltz, J.J. Eidel, AAPG Memoir 51, p. 101-107.

MUNNECKE, A., Samtleben, C., and Bickert, T., 2003. The Ireviken Event in the Lower Silurian of Gotland, Sweden - Relation to similar Palaeozoic and Proterozoic events. Palaeogeography, Palaeoclimatology, Palaeoecology 195, p. 99-124.

MUNNECKE, A., and Männik, P., 2009. New biostratigraphic and chemostratigraphic data from the Chicotte Formation (Llandovery, Anticosti Island, Laurentia) compared with the Viki core (Estonia, Baltica). Estonian Journal of Earth Sciences 58, p. 159-169.

MUNNECKE, A., Calner, M., Harper, D.A.T., and Servais, T., 2010. Ordovician and Silurian sea-water chemistry, sea level, and climate: A synopsis. Palaeogeography, Palaeoclimatology, Palaeoecology 296, p. 389-413.

MYROW, P.M., 1992. Pot and gutter casts from the Chapel Island Formation southeast Newfoundland. Journal of Sedimentary Petrology, Vol. 62, p. 992-1007.

NANCE, R.D., and Linnemann, U., 2008.The Rheic Ocean: origin, evolution and significance. GSA Today, Vol. 18, n° 12.

NESTOR, H., Copper, P., and Stock, C., 2010. Late Ordovician and Early Silurian stromatoporoid sponges from Anticosti Island, Eastern Canada: crossing the O/S mass exctinction boundary. NRC Research Press, Ottawa.

PAGE, A., Zalasiewicz, J., Williams, M., and Popov, L., 2007. Were transgressive black shales a negative feedback modulating glacioeustasy in the Early Palaeozoic Icehouse? *In* Deep-Time Perspectives on Climate Change: Marrying the Signal from Computer Models and Biological Proxies: Special Publication of the Geological Society of London, *edited by* M. Williams, A.M. Haywood, F.J. Gregory, D.N. Schmidt. The Micropalaeontological Society, p. 123-156.

PÉREZ-LÓPEZ, A., and Pérez-Valera, F., 2011. Tempestite Facies Models for the Epicontinental Triassic Carbonates of the Betic Cordillera (Southern Spain). Sedimentology 59, p. 646-678.

PETYK, A.A., 1981. Lithostratigraphie, paléogéographie et potentiel en hydrocarbure de l'Île d'Anticosti. Ministère Energie Ressources, Québec.

PINET, N., 2011. Hinterland-directed transtensional faulting at an orogen structural front: the example of the Cap-Chat mélange, Quebec Appalachians. GSA Bulletin, Vol. 123, n° 11/12, p. 2256-2265.

PLINT, A.G., 2010. Wave- and storm-dominated shoreline and shallow marine systems. *In* Facies Models 4, *edited by* N.P. James and R.W. Dalrymphe, Geological Association of Canada, p. 137-199.

POSAMENTIER, H., and Allen, G. 1999, Siliciclastic sequence stratigraphy - concepts and applications. SEPM Concepts in Sedimentology and Paleontology, Vol. 7.

PRATT, B.R., James, N.P., and Cowan, C.A., 1994. Peritidal carbonates. In Facies Models – Response to sea level change, *edited by* R.G. Walker and N.P. James. Geological Association of Canada, p. 303-322.

RICHARDSON, J., 1857. Report for the year 1856. Geological Survey of Canada, Report of Progress for the Years 1853-54-55-56, Ottawa, p. 191-245.

RUDDIMAN W.F., 2008. Earth's climate past and future, 2nd edition. Basingstoke: W.H. Freeman and Co.

SAMI, T., and Desrochers, A., 1992. Episodic sedimentation on an Early Silurian storm-dominated carbonate ramp, Becscie and Merrimack Formations, Anticosti Island, Canada. Sedimentology, Vol. 39, p. 355-381.

SCHUCHERT, C., and Twenhofel, W.H., 1910. Ordovicic-Siluric section of the Mingan and Anticosti Islands, Gulf of St. Lawrence. Geological Society of America, Bulletin, Vol. 21, p. 677-716.

SCOTESE, C.R., 1997. Paleogeographic atlas. Paleomap Progress Report 90-0497, Department of Geology, University of Texas, Arlington, Texas.

SOQUIP and Petro-Canada.1987. Estuary and gulf of St-Lawrence geological, geophysical, geochemical data integration. Geological Survey of Canada, Open file 1721. Shuttle Radar Topography Mission (SRTM). 2000. Digital Elevation Model, Finished 3 arc sec. Shaded relief (90 meter resolution). Distributed by USGS (United States Geological Survey) via the Seamless Distribution System.

SPENGLER, A.E., and Read, J.F., 2010. Sequence Development on a Sediment-starved, Low Accommodation Epeiric Carbonate Ramp: Silurian Wabash Platform, USA Mid-Continent during Icehouse to Greenhouse Transition. Sedimentary Geology 224, p. 84-115.

TWENHOFEL, W.H., 1928. Geology of Anticosti Island. *In* Geological Survey of Canada, Memoir 154.

TUCKER, M.E., 1988. Techniques in sedimentology. Blackwell science, Oxford.

UYENO, T.T., and BARNES, C.R., 1981. A summary of Lower Silurian conodont biostratigraphy of the Jupiter and Chicotte formations, Anticosti Island, Québec. *In* IUGS Subcommission on Silurian Stratigraphy, Ordovician-Silurian Boundary Working Group, *edited by* Lespérance P.J. Field Meeting, Anticosti-Gaspé, Québec, 1981, Volume II: Stratigraphy and Paleontology. Departement de Géologie, Université de Montréal, Montréal, p. 173-184.

WENZEL, B., and Joachimski, M.M., 1996. Carbon and oxygen isotopic composition of Silurian brachiopods (Gotland/Sweden): paleoceanographic implications. Palaeogeography, Palaeoclimatology, Palaeoecology 122, p. 143-166.

YANG, B., Dalrymphe, R.W., and Chun, S., 2006. The significance of hummocky cross-stratification (HCS) wavelengths: evidence from an open-coast tidal flat, South Korea. Journal of Sedimentary Research, Vol. 76, p. 2-8.

	Loss On	Sum	SiO_2	Al_2O_3	CaO	K_2O	MgO	MnO	Na_2O	P_2O_5	$Fe_2O_{3(T)}$	Zn	TiO_2	Ba	Co
Sample name	(%)	(%)	(%)	(%)	(%)	(%)	(%)	(%)	(%)	(%)	(%)	(ppm)	(%)	(ppm)	(ppm)
DR-N	2.26	97.11	52.67	17.44	6.93	1.69	4.23	0.22	2.86	0.23	9.63	136	1.05	375	39
BCR-2	0.50	98.93	53.49	13.28	7.06	1.76	3.42	0.20	2.93	0.35	13.00	127	2.24	655	41
FC-1	16.00	84.98	44.97	12.74	12.26	2.90	5.16	0.05	0.83	0.11	5.18	64	0.63	314	19
FC-2	8.30	92.62	54.29	16.72	2.35	3.32	5.47	0.05	1.47	0.11	7.89	75	0.80	378	30
FC-3	6.00	93.69	54.72	17.52	1.19	7.19	3.94	0.04	0.64	0.08	7.40	72	0.81	454	24
FC-4	13.10	87.44	46.36	13.83	9.10	5.42	4.73	0.05	0.58	0.08	6.43	51	0.72	415	22
FC-5	8.30	91.75	53.02	19.92	3.40	5.75	2.53	0.03	0.29	0.06	5.73	68	0.88	436	24
FC-6	17.80	84.05	43.29	11.43	17.42	5.04	2.62	0.03	0.16	0.04	3.41	40	0.50	263	16

	Ga	La	Ni	Pb	Rb	Sr	Th	U	V	Y	Zr	Nb	Cr	Ce	Nd
Sample name	(ppm)	(ppm)	(ppm)	(ppm)	(ppm)	(ppm)	(ppm)	(ppm)	(ppm)	(ppm)	(ppm)	(ppm)	(ppm)	(ppm)	(ppm)
DR-N	14	25	10	66	68	378	11	3	204	25	142	7	37	42	17
BCR-2	14	26	4	13	46	328	14	5	394	33	180	12	32	9	10
FC-1	10	43	60	14	105	446	13	1	89	12	135	11	113	41	7
FC-2	5	18	141	36	118	91	38	18	125	14	135	14	187	42	9
FC-3	16	34	109	20	158	60	25	11	115	13	155	13	175	27	10
FC-4	4	13	70	46	129	81	37	17	86	13	142	13	115	56	23
FC-5	19	40	44	35	198	104	28	12	130	17	130	18	97	54	17
FC-6	-1	1	24	45	114	143	32	12	85	10	97	14	74	48	18

Appendix 1: XRF data

Appendix 2: XRD Spectra. XRD data are considered to be not relevant as we are missing a critical range of diffraction angles (from 2° to 10°) to determine the clay minerals. Nevertheless, it confirms the presence of two groups: a carbonate-rich and a carbonate-poor. Abbreviations indicate the interpreted minerals: Qz = quartz; Or = orthoclase; Al = albite; Ca = calcite; An = ankerite; Do = dolomite; Sm = smectite; Ka = kaolinite; Ch = chlorite.

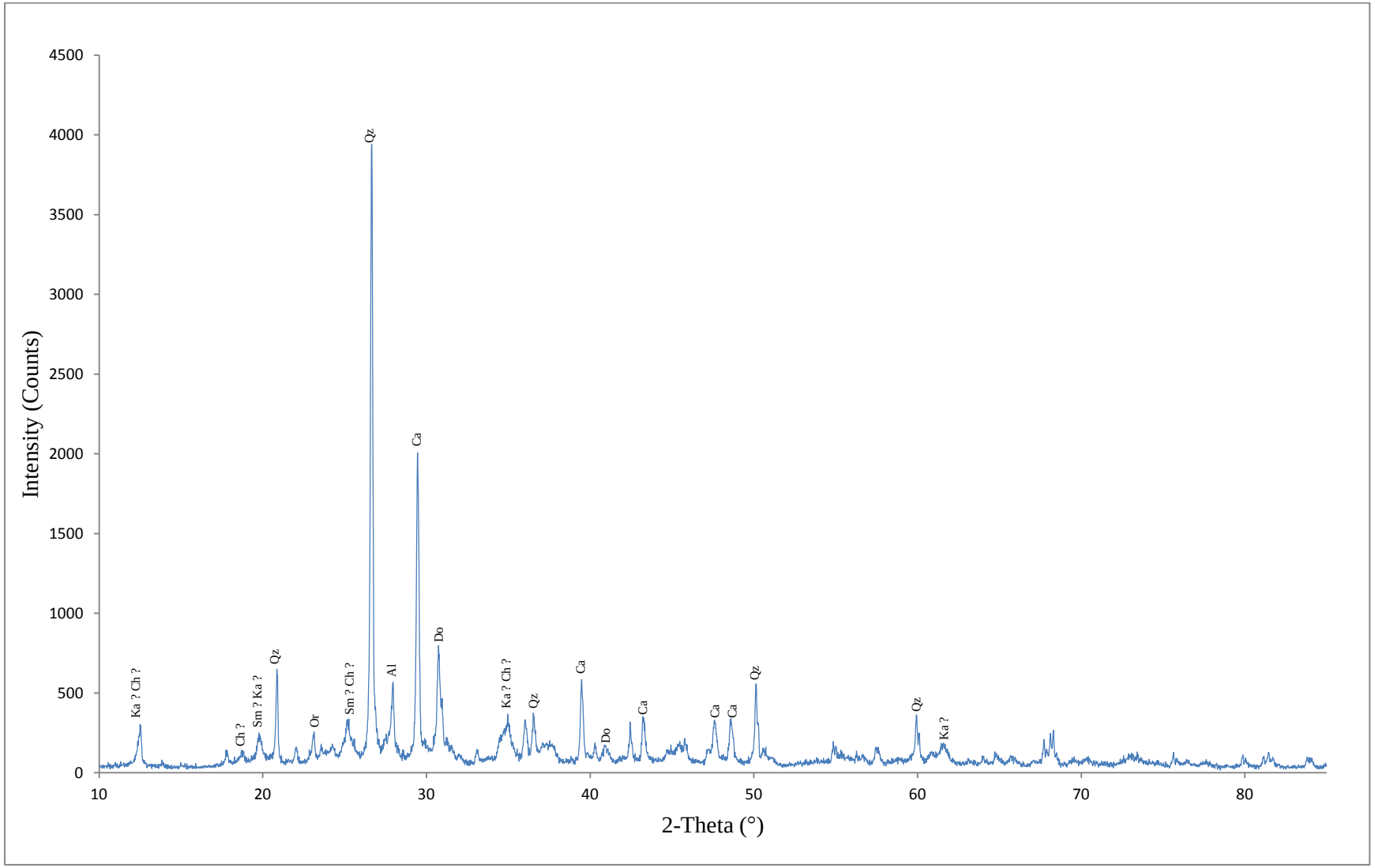

Appendix 2a: XRD spectrum of FC-1 from the Ellis Bay Formation (Late Ordovician)

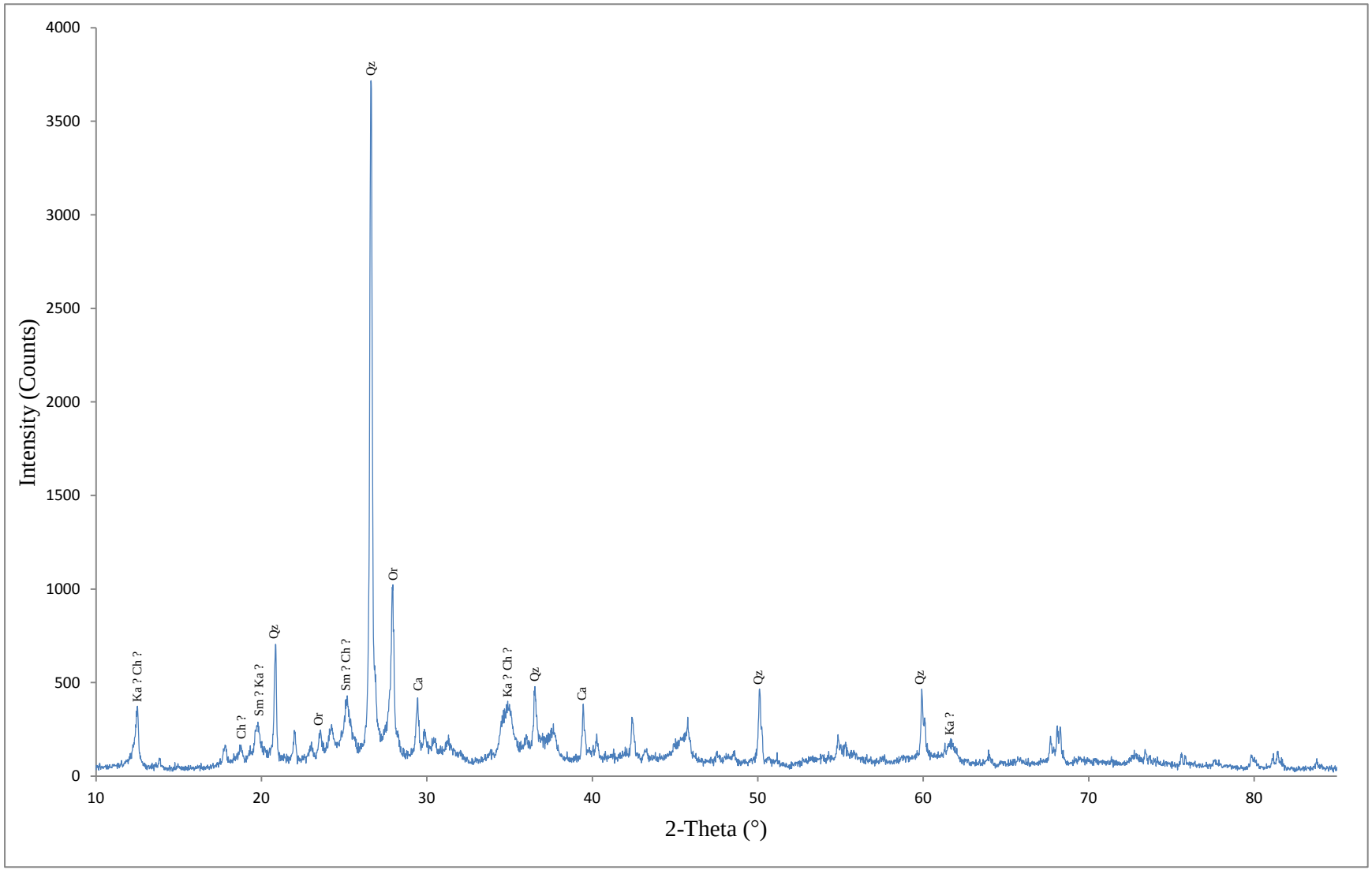

Appendix 2b: XRD spectrum of FC-2 from the Merrimack Formation (Rhuddanian)

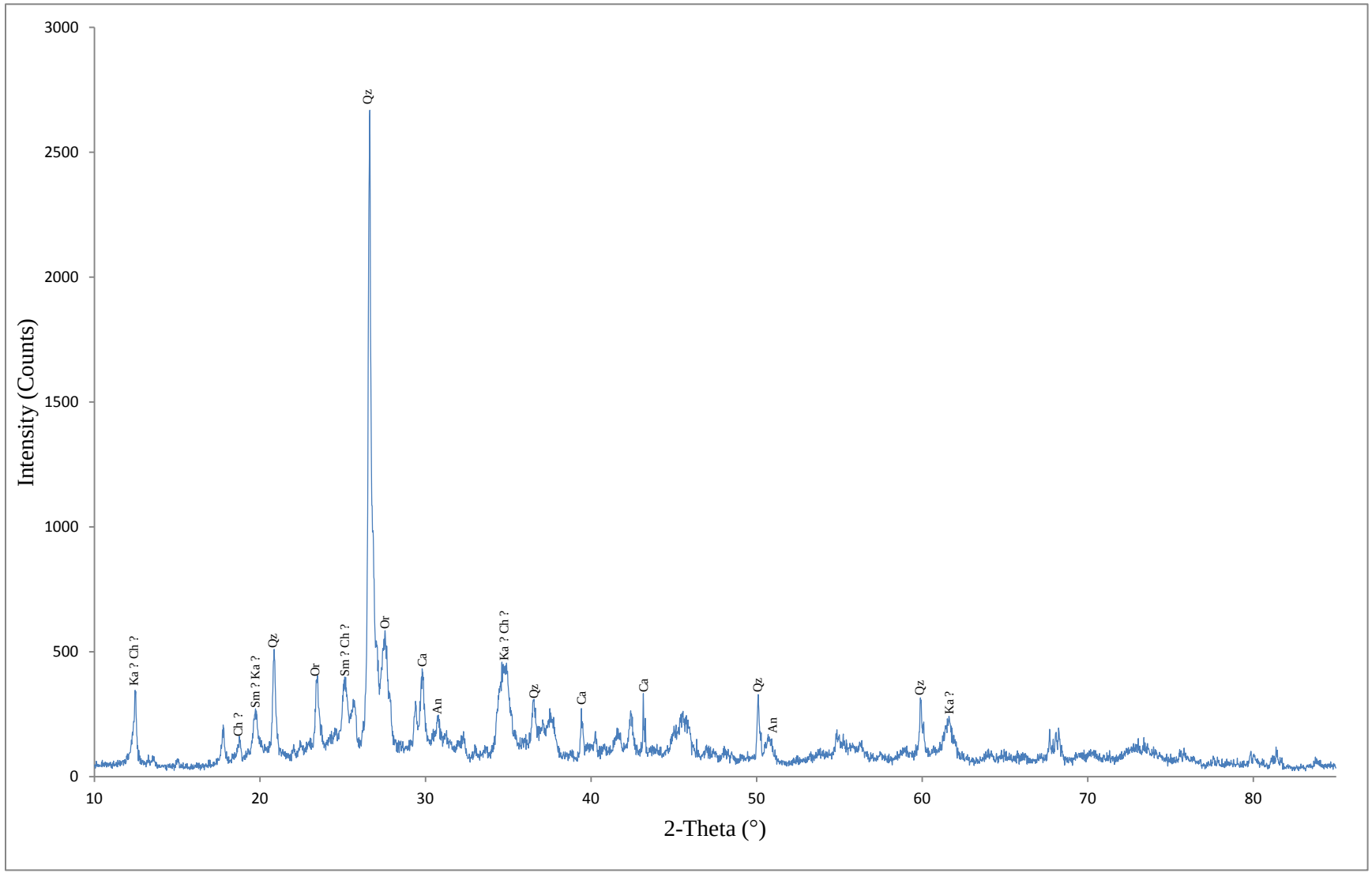

Appendix 2c: XRD spectrum of FC-3 from the Jupiter Formation (Section 1: 8.5 m above the base)

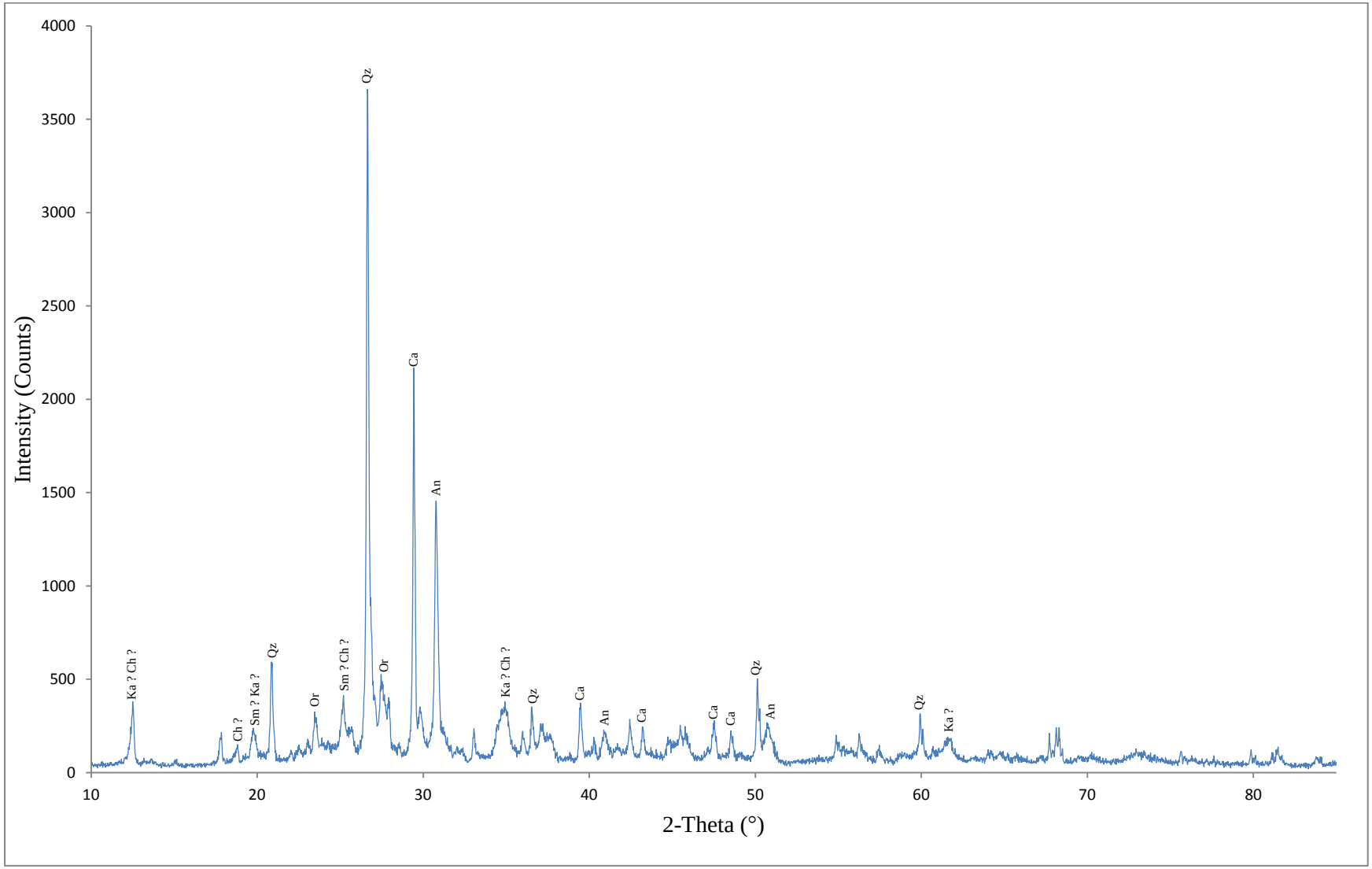

Appendix 2d: XRD spectrum of FC-4 from the Jupiter Formation (Section 3: 1.5 m above the base)

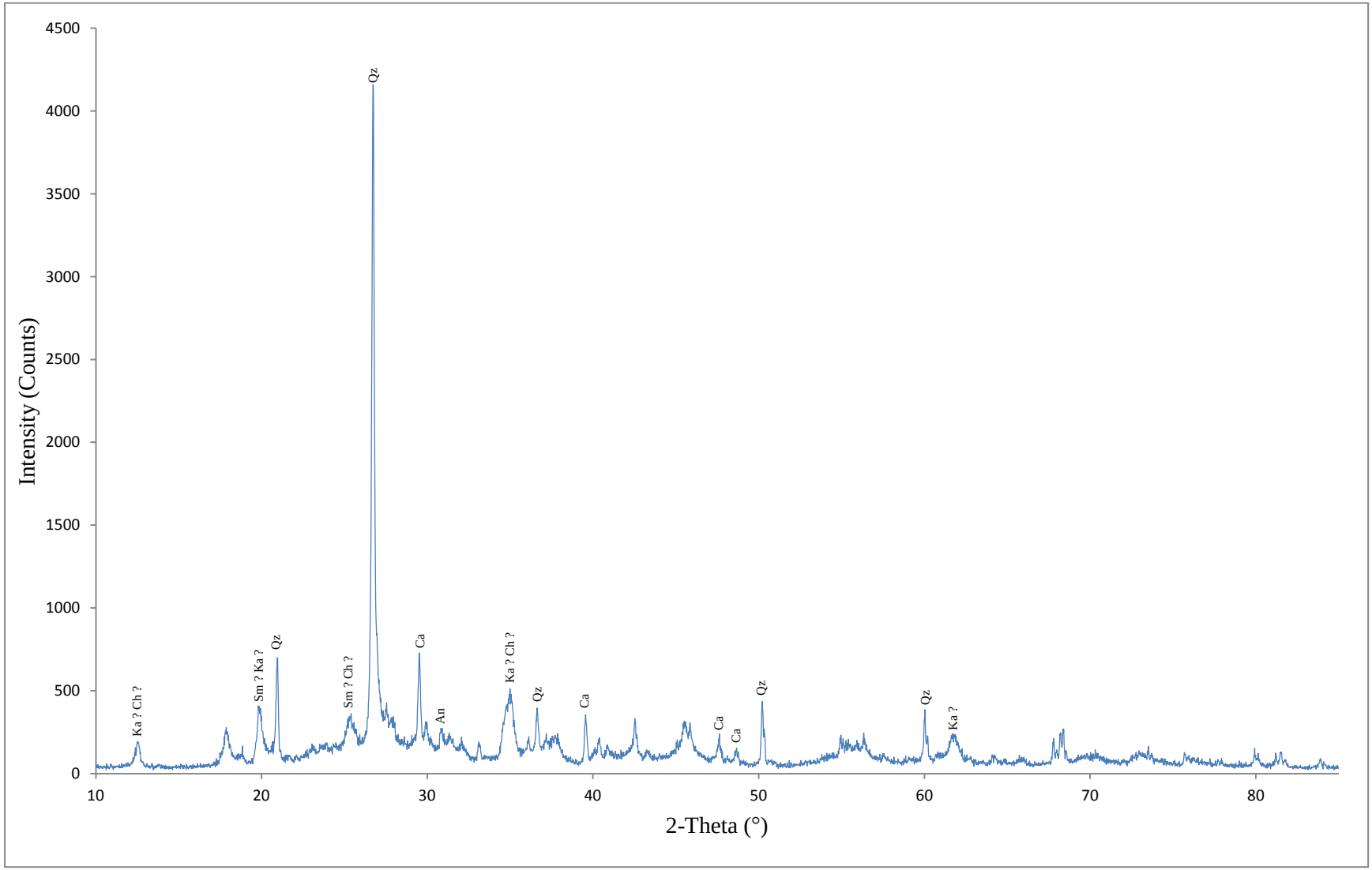

Appendix 2e: XRD spectrum of FC-5 from the Jupiter Formation (Section 4: 3.5 m above the base)

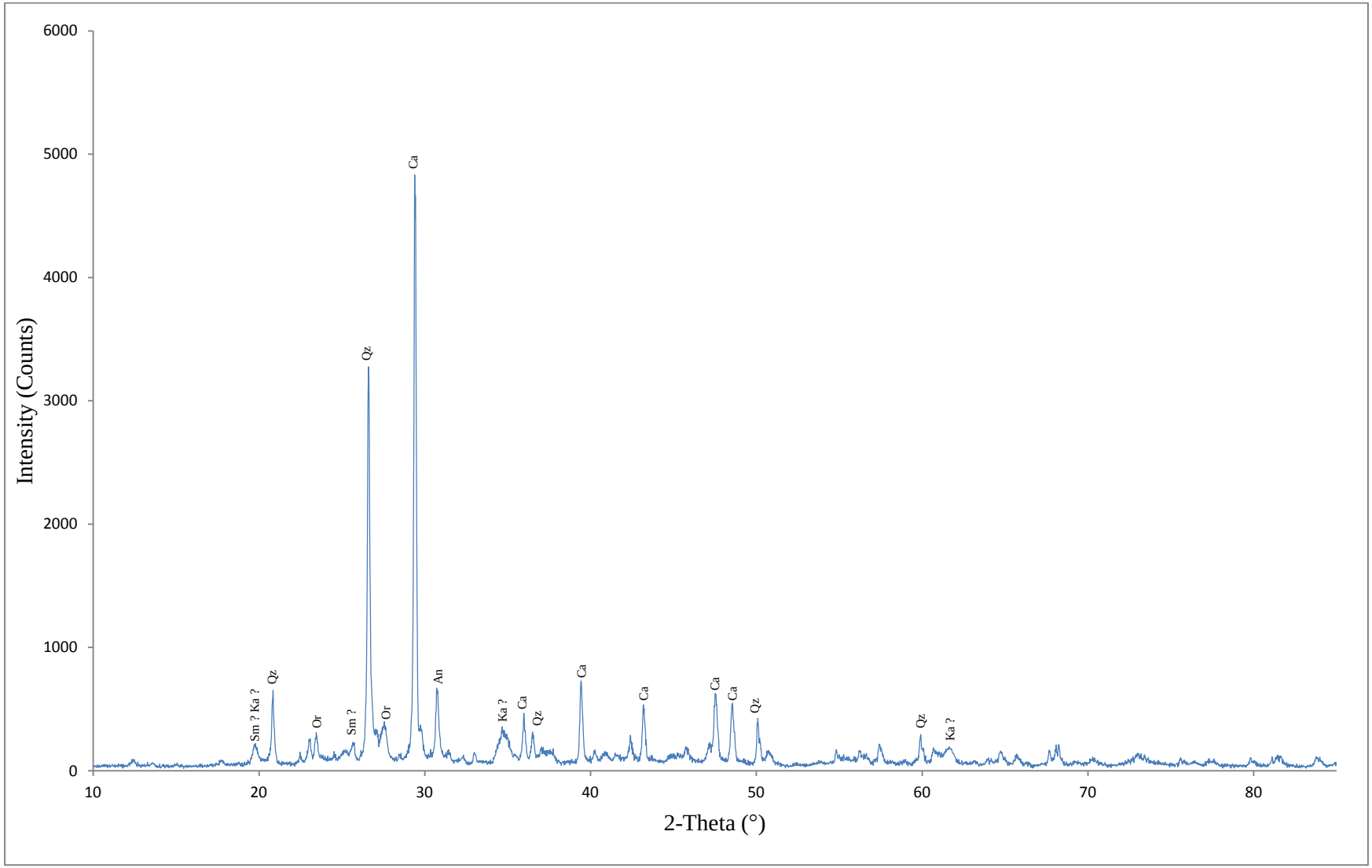

Appendix 2f: XRD spectrum of FC-6 from the Chicotte Formation (Section 4: 12.5 m above the base)